The C-terminal domain of LRRK2 with the G2019S mutation is sufficient to produce neurodegeneration of dopaminergic neurons in vivo

Noémie Cresto, Marie-Claude Gaillard, Camille Gardier, Francesco Gubinelli, Elsa Diguet, Déborah Bellet, Laurine Legroux, Julien Mitja, Gwenaëlle Auregan, Martine Guillermier, et al.

Neurobiology of Disease 134 (2020) 104614

Contents lists available at ScienceDirect

Neurobiology of Disease

journal homepage: www.elsevier.com/locate/ynbdi

The C-terminal domain of LRRK2 with the G2019S mutation is sufficient to produce neurodegeneration of dopaminergic neurons *in vivo*

Noémie Cresto[a,b], Marie-Claude Gaillard[a,b], Camille Gardier[a,b], Francesco Gubinelli[a,b], Elsa Diguet[a,b,c], Déborah Bellet[a,b], Laurine Legroux[a,b], Julien Mitja[a,b], Gwenaëlle Auregan[a,b], Martine Guillermier[a,b], Charlène Josephine[a,b], Caroline Jan[a,b], Noëlle Dufour[a,b], Alain Joliot[d], Philippe Hantraye[a,b], Gilles Bonvento[a,b], Nicole Déglon[a,e,f], Alexis-Pierre Bemelmans[a,b], Karine Cambon[a,b], Géraldine Liot[a,b], Emmanuel Brouillet[a,b,*]

[a] CEA, DRF, Institut de Biologie Françoise Jacob, Molecular Imaging Research Center (MIRCen), F-92265 Fontenay-aux-Roses, France
[b] CNRS, CEA, Paris-Sud Univ., Univ. Paris-Saclay, Neurodegenerative Diseases Laboratory (UMR9199), F-92265 Fontenay-aux-Roses, France
[c] Institut de Recherche SERVIER, Neuropsychiatry Department, 125 chemin de ronde, 78290 Croissy sur Seine, France
[d] Homeoprotein and Plasticity, Center for Interdisciplinary Research in Biology (CIRB), College de France, CNRS, INSERM, PSL Research University, Paris, France
[e] Lausanne University Medical School (CHUV), Department of Clinical Neurosciences (DNC), Laboratory of Cellular and Molecular Neurotherapies (LNCM), Lausanne, Switzerland
[f] Lausanne University Medical School (CHUV), Neuroscience Research Center (CRN), Laboratory of Cellular and Molecular Neurotherapies (LNCM), Lausanne, Switzerland

ARTICLE INFO

Keywords:
Parkinson's disease
Leucine-rich repeat kinase 2
Lentiviral vectors
AAVs

ABSTRACT

The G2019S substitution in the kinase domain of LRRK2 (LRRK2^{G2019S}) is the most prevalent mutation associated with Parkinson's disease (PD). Neurotoxic effects of LRRK2^{G2019S} are thought to result from an increase in its kinase activity as compared to wild type LRRK2. However, it is unclear whether the kinase domain of LRRK2^{G2019S} is sufficient to trigger degeneration or if the full length protein is required. To address this question, we generated constructs corresponding to the C-terminal domain of LRRK2 (ΔLRRK2). A kinase activity that was increased by G2019➔S substitution could be detected in ΔLRRK2. However biochemical experiments suggested it did not bind or phosphorylate the substrate RAB10, in contrast to full length LRRK2. The overexpression of ΔLRRK2^{G2019S} in the rat striatum using lentiviral vectors (LVs) offered a straightforward and simple way to investigate its effects in neurons *in vivo*. Results from a RT-qPCR array analysis indicated that ΔLRRK2^{G2019S} led to significant mRNA expression changes consistent with a kinase-dependent mechanism. We next asked whether ΔLRRK2 could be sufficient to trigger neurodegeneration in the substantia nigra *pars compacta* (SNc) in adult rats. Six months after infection of the substantia nigra pars compacta (SNc) with LV-ΔLRRK2^{WT} or LV-ΔLRRK2^{G2019S}, the number of DA neurons was unchanged. To examine whether higher levels of ΔLRRK2^{G2019S} could trigger degeneration we cloned ΔLRRK2 in AAV2/9 construct. As expected, AAV2/9 injected in the SNc led to neuronal expression of ΔLRRK2^{WT} and ΔLRRK2^{G2019S} at much higher levels than those obtained with LVs. Six months after injection, unbiased stereology showed that AAV-ΔLRRK2^{G2019S} produced a significant ~30% loss of neurons positive for tyrosine hydroxylase- and for the vesicular dopamine transporter whereas AAV-ΔLRRK2^{WT} did not. These findings show that overexpression of the C-terminal part of LRRK2 containing the mutant kinase domain is sufficient to trigger degeneration of DA neurons, through cell-autonomous mechanisms, possibly independent of RAB10.

Abbreviations: ΔLRRK2, ROC-COR-kinase plus the WD40 domain; AAV, adeno-associated virus; ANK, Ankyrin; ANOVA, analysis of variance; ARM, Armadillo; ATP, Adenosine triphosphate; BSA, Bovine serum albumin; BCA, bicinchoninic acid assay; CamKII, Calmodulin-kinase II; COR, C-terminal of ROC; DA, Dopaminergic; DAB, Diaminobenzidine; DLU, Density light unit; DK, double-mutant G2019S/D1994A dead kinase; GFP, Green fluorescent protein; GS, G2019S mutation; GWAS, Genome-wide association studies; HA, Hemagglutinin tag; K, Kinase domain of LRRK2; KB1, Kinase buffer 1 (20 mM HEPES, 150 mM NaCl, 5 mM EGTA, 20 mM β-glycerophosphate); KB2, Kinase buffer 2 (10 mM ATP, 20 mM MgCl2); LB, Lysis buffer (50 mM Tris, pH 8.0, 150 mM NaCl, 1 mM EDTA, 0.5% Triton X-100, 1% NP40, protease inhibitors); LRR, Leucin-rich repeats; LRRK2, Leucin-rich repeats kinase 2; LV, Lentivirus; MBP, Myelin basic protein; PAGE, Poly-Acrylamide Gel Electrophoresis; PBS, Phosphate buffer saline; PBS-T, Phosphate Buffer Saline with 0.2% Triton X-100; PD, Parkinson's disease; RCK, Kinase domain plus the ROC-COR domain; ROC, Ras-of-complex protein; SDS, Sodium-dodecyl-Sulfate; SNc, Substantia nigra *pars compacta*; SNPs, single-nucleotide polymorphisms; TBS, Tris Buffer Saline; TBS-T, Tris Buffer Saline with 0.1% Tween-20; TH, Tyrosine hydroxylase; WT, Wild-type

* Corresponding author at: CEA, DRF, Institut de Biologie Françoise Jacob, Molecular Imaging Research Center (MIRCen), F-92265 Fontenay-aux-Roses, France.
E-mail address: emmanuel.brouillet@cea.fr (E. Brouillet).

https://doi.org/10.1016/j.nbd.2019.104614
Received 12 March 2019; Received in revised form 4 September 2019; Accepted 16 September 2019
Available online 09 October 2019

1. Introduction

Parkinson's disease (PD) is a neurodegenerative disorder affecting approximately seven million people worldwide. It is characterised by motor symptoms (rigidity, bradykinesia, resting tremors, gait instability) and a large spectrum of non-motor symptoms (*e.g.* dysosmia, sleep disorder, dementia) (Poewe, 2008; Rodriguez-Oroz et al., 2009). The neuropathological hallmarks of PD are a progressive loss of dopaminergic (DA) neurons in the substantia nigra *pars compacta* (SNc) and the presence of neuronal inclusions (Lewy bodies) and dystrophic neurites containing aggregated α-synuclein protein (Braak and Braak, 2000). The cause of DA neuron degeneration is poorly understood. PD is mostly sporadic, but a genetic origin can be found in about 10% of cases. Several genes are known to be associated with familial (or *de novo* genetic) forms of PD (Lesage and Brice, 2009).

Mutations in the *LRRK2* (Leucine-Rich Repeat Kinase 2) gene are the most common genetic cause of both familial and sporadic PD (Paisán-Ruíz et al., 2004). Genome-wide association studies (GWAS) have also identified single-nucleotide polymorphisms (SNPs) at the *LRRK2* locus significantly associated with an increase or a decrease in the risk of developing PD, consistent with a key role for LRRK2 in PD pathogenesis (Nalls et al., 2014; Satake et al., 2009). It has also recently been shown that LRRK2 was activated (increased autophosphorylation and increased phosphorylation of its substrate RAB10) in the SNc of sporadic PD patients (Di Maio et al., 2018). The most prevalent pathogenic mutation of LRRK2 is the G2019S substitution (Gilks et al., 2005; Healy et al., 2008).

The mechanisms underlying the neurotoxicity of the G2019S mutant LRRK2 protein ($LRRK2^{G2019S}$) are unknown (Cresto et al., 2019). *LRRK2* gene encodes a large 2527-amino acid multidomain protein. The pathogenic mutations of *LRRK2* are clustered in the central region encoding the three domains forming the catalytic (kinase) core of the protein (Cookson, 2010; Mata et al., 2006). The G2019S mutation affects an amino acid located in this kinase domain. LRRK2 belongs to the ROCO protein family, and bears the tandem Ras-of-complex proteins (Roc), GTPase and C-terminal of Roc (COR) domains characteristic of this family. LRRK2 also has regions involved in protein-protein interactions [ankyrin (ANK), armadillo (ARM), leucine-rich repeats (LRR)] at its N-terminal and a WD40 domain at its C-terminal, suggesting a possible function as a scaffolding protein. The G2019S mutation increases LRRK2 kinase activity (both auto-phosphorylation and the phosphorylation of substrates) and there is compelling evidence to suggest that the neurotoxicity of $LRRK2^{G2019S}$ is linked to an increase in the kinase activity of this protein (Lee et al., 2010; West et al., 2007). Recent results obtained in transgenic mice expressing LRRK2 in non-dopaminergic neurons show that full length $LRRK2^{G2019S}$ is no longer neurotoxic when its kinase domain is inactivated (*e.g.* D1994E mutation), which demonstrates that the activity of the kinase domain is crucial for toxicity (Xiong et al., 2017). In support of this, a number of studies showed that pharmacological inhibitors of the kinase can produce neuroprotection against mutant LRRK2 (for a review see Cresto et al., 2019). However, it is unclear whether the kinase domain of $LRRK2^{G2019S}$ is sufficient to trigger degeneration or if the full length protein is required. Several reports indicated that truncated fragments of LRRK2 can produce cellular changes that depend on the activity of the kinase domain, indicating that the entire protein may not be required to trigger some of LRRK2 signalling/biological functions (Aufschnaiter et al., 2018; Pereira et al., 2014; Sheng et al., 2010). This question is not purely theoretical. It may have practical implications. Especially, apart from existing compounds that produce LRRK2 kinase inhibition, other types of strategies (peptide, aptamers *etc.*…) selectively impeaching the interaction of the kinase domain with its substrates (without interfering with non-kinase-dependent LRRK2 functions associated with the N-terminal domain for example) may also be of interest.

The role of the LRRK2 kinase domain in dopaminergic (DA) neurons has rarely been studied *in vivo*. Transgenic and knock-in genetic models expressing $LRRK2^{G2019S}$ have been developed in rodents. These animals display very progressive motor deficits, subtle defects in striatal DA release, but little or no DA neuron loss, even at two years of age (Beccano-Kelly et al., 2014; Lee et al., 2015; Ramonet et al., 2011; Yue et al., 2015). This is likely due to the low expression of LRRK2 in DA neurons is these models. Double transgenic mice expressing high levels of LRRK2 under the control of the CamKII and Tet promoters show progressive degeneration of neurons in the cortex and striatum (Lin et al., 2009), whereas the SNc is spared since CamKII induces minimal expression in DA cells. Of major interest, a recent report showed that expression of $LRRK2^{G2019S}$ under the control of the TH promoter leads to robust degeneration of DA neurons and a severe behavioural phenotype (Xiong et al., 2018). These results suggest that high levels of $LRRK2^{G2019S}$ expression are required to trigger cell death in the SNc. In support of this hypothesis, intrastriatal injection of an HSV amplicon (HSV) and an adenovirus (Adeno) encoding $LRRK2^{G2019S}$ in the mouse and rat striatum respectively, produces a partial but relatively rapid degeneration of DA neurons (Dusonchet et al., 2011; Lee et al., 2010). It was also shown recently that overexpression of $LRRK2^{G2019S}$ in SNc after injection of canine-Adeno viral vectors (CAV2) in the striatum leads to partial degeneration of dopaminergic neurons in the SNc in the primate *Microcebus murinus* (Mestre-Francés et al., 2018). Although these vectors do not transduce DA neurons alone (striatal neurons and astrocytes are transduced as well), these new studies demonstrate that local brain infection with viral vectors might be a versatile approach to study mutant LRRK2 pathophysiology *in vivo* in different animal species.

Here, we investigated whether an increase in the kinase activity of $LRRK2^{G2019S}$ selectively in DA neurons could lead to cell-autonomous neurodegeneration. We addressed this question *in vivo,* in the context of the DA neurons of the SNc in rats. We used lentiviral vectors (LVs) and adeno-associated viruses (AAV2/9), which can overexpress transgenes selectively in neurons. In this study, we generated lentiviral vectors (LVs) encoding the C-terminal part [1326–2527 a.a., called hereafter "ΔLRRK2"] of the wild-type ($\Delta LRRK2^{WT}$), G2019S mutant ($\Delta LRRK2^{G2019S}$) or double-mutant G2019S/D1994A dead kinase ($\Delta LRRK2^{DK}$) forms of LRRK2. Since our results showed that LV-mediated overexpression of ΔLRRK2 produced no significant toxicity in dopaminergic neurons *in vivo*, we generated AAV2/9 encoding ΔLRRK2 fragments and tested the potential neurotoxic effects of these AAVs after their stereotaxic injection into the SNc of adult rats. Effects of vectors coding ΔLRRK2 were mainly evaluated using behavioural motor tests and histological evaluation of the nigro-striatal pathway (See Supplementary Fig. S1 for general design of *in vivo* experiments in rats).

2. Materials and methods

2.1. Viral construction and production

2.1.1. Lentivirus

DNA sequences encoding GFP and the C-terminal part of human LRRK2 (kinase, K; ROC-COR-kinase, RCK; RCK plus the WD40 domain, called hereafter "ΔLRRK2") were synthesised and inserted into the self-inactivated vector (SIN) backbone containing the WPRE element (W) and the murine ubiquitous phosphoglycerate kinase 1 promoter (PGK). We generated lentivirus vectors LV-GFP, and LV-ΔLRRK2 coding for the WT form or G2019S forms of the fragments. Viral particles were produced as described elsewhere (Hottinger et al., 2000). All the SIN vectors were pseudotyped with VSVg glycoprotein G. Briefly, the viral particles were produced in HEK-293 T cells by a four plasmid transient transfection system (Naldini et al., 1996). The supernatant was collected 48 h later and filtered, and the particle content of the viral batches was determined by ELISA for the p24 antigen (Gentaur, Paris, France). High-titre stocks were obtained by ultracentrifugation. The pellet was re-suspended in 1% BSA in PBS, frozen and stored at −80 °C.

LV-ΔLRRK2 vectors were used at a concentration of 100 ng/μl p24.

Adeno-associated viral vector (AAV). Plasmid constructs were packaged into AAV2/9 capsids as described previously (Berger et al., 2015). Briefly, viral particles were produced by co-transfection of HEK-293 T cells with (1) an adenovirus helper plasmid (pXX6–80), (2) an AAV and expressed as viral genomes per ml of concentrated stocks (Vg/ml) (Aurnhammer et al., 2012).

2.2. Cell studies

Human embryonic kidney 293T cells (HEK293T) were grown at 37 °C in Dulbecco's modified Eagle's medium supplemented with 10% bovine calf serums, under an atmosphere containing 5% CO_2. For the study of recombinant ΔLRRK2, cultured cells were seeded on wells and transfected by calcium phosphate transfection methods with the different forms of ΔLRRK2 vectors. For RAB10 immunoprecipitation studies with the ΔLRRK2 fragments, a stable HEK 293T cell line was generated using lentivirus infection. The ΔLRRK2 cell lines (LacZ, WT, GS, DK) were maintained as the parental HEK described just above.

2.3. Biochemical analysis

2.3.1. Western blotting

Overall levels of fragment expression were determined by lysing cells in modified RIPA buffer (without SDS): 50 mM Tris, pH 8.0, 150 mM NaCl, 1 mM EDTA, 0.5% Triton X-100, 1% NP40 and protease inhibitor cocktail (Roche). Cell lysates were centrifuged at 13,000 x*g* for 20 min at 4 °C. The supernatant was collected, and dispensed into aliquots, which were stored at −80 °C to prevent degradation. A fraction was retained for the determination of total protein concentration with a BCA kit (Pierce). Equal amounts of total protein extract were subjected to SDS–PAGE in 4 to 12% Bis–Tris gels (NuPAGE Novex Bis-Tris midi gel; 15 or 26 wells, Invitrogen) and the bands were transferred to nitrocellulose membranes. The membranes were blocked (5% milk in TBS–0.1% Tween-20) and incubated overnight with primary antibodies against actin (1:5000, rabbit, Sigma), and, for the detection of transgenes, with antibodies against HA (1:3000, mouse, Covance). The membranes were washed three times, with 0.1% Tween-20 in TBS (TBS-T), for 10 min each. For chemo-luminescence-based detection, membranes were labelled for 1 h with secondary IgG-HRP antibodies raised against the corresponding primary antibodies. The membranes were washed three times with TBS-T and incubated with ECL chemoluminescence reagent (Clarity Western ECL substrate; Bio-Rad), according to the supplier's instructions. Peroxidase activity was detected with the Fusion TX7 camera system (Fisher Scientific). Signals were normalized against the actin signal, by densitometry analysis with ImageJ software. For fluorescence-based detection, membranes were labelled for 1 h with secondary IgG-coupled with fluorescents dyes (Li-cor Biosciences, Germany). The fluorescent signal was then visualized using Odyssey CLx Imager (Li-cor Biosciences, Germany) and analysis performed using Image Studio software (Li-cor Biosciences, Germany).

2.3.2. Immunoprecipitation of LRRK2-HA fragments

Lysates of transfected HEK cells were used for the immunoprecipitation protocol. In total, 750 μg protein, as determined with the BCA kit, was mixed in 500 μl of lysis buffer (LB) and a 1:150 dilution of HA antibody was added. The mixture was incubated overnight at 4 °C, with 360° rotation, to allow the protein-antigen complex to form. The next day, 20 μl of magnetic beads coated with protein A/G (Dynabeads NOVEX, Life Technologies) were washed three times in LB. The tube containing the beads was placed on a magnet, causing the beads to migrate to the side of the tube facing the magnet, thereby facilitating supernatant removal. The protein-antigen complex was added to the beads, and the mixture was incubated at room temperature for 2 h to allow the bead-Ab-Ag complex to form. The supernatant was removed and the beads were washed three times in LB.

2.3.3. Immunoprecipitation of RAB10

Lysates of HEK stable cells for ΔLRRK2 or calcium phosphate transfected HEK cells for full length LRRK2 were obtained using a lysis buffer (LB; 50 mM Tris pH 8.0, 150 mM NaCl, 1% NP-40, 1 mM PMSF, 1% protease inhibitor cocktail and 1% phosphatase inhibitor cocktail). Lysate was centrifuged at 15000 *g* for 10 min at 4 °C and supernatant was collected to perform a total protein assay (BCA kit). Magnetic beads coated with protein A/G (Dynabeads NOVEX, Life Technologies) were incubated with 2 μl (=1 μg) of RAB10 antibody during 1 h at 4 °C. Next, 30 μl of this complex RAB10 Antibody/magnetic beads was incubated with 500 μg of total proteins in 500 μl of lysis buffer during 2 h at 4 °C on rotation. After 3 washes with the lysis buffer, proteins were denaturated with Laemmli buffer and submitted to SDS-PAGE in 4–20% Tris-Glycine gels (Bio-Rad). Detection of corresponding western blots was performed with: anti RAB10 Ab (Abcam), anti-phosho-RAB10 T73 (Abcam), anti-HA (Covance), anti-Actin (Sigma), anti-tubulin (Sigma). The secondary antibody used for detection of Rab10 and Phospho-RAB10 was the Clean-Blot IP Detection Reagent-HRP (Thermo Fisher).

2.3.4. Kinase activity assay

The lysate buffer (LB) was removed and the beads-Ab-Ag complex was resuspended in 30 μl of kinase buffer (KB1: 20 mM HEPES; 150 mM NaCl, 5 mM EGTA; 20 mM beta-glycerophosphate). The mixture was split into two samples (10 μl and 20 μl), one for estimation of the amount of protein (non-radioactive fraction) and the other for a phosphorylation activity assay with MBP. For measurements of phosphorylation activity, we added 5 μl of KB2 (10 mM ATP, 20 mM $MgCl_2$) and 5 μCi ^{32}P-ATP (1 mCi, BLU502Z001MC, PerkinElmer) to activate the reaction, and the mixture was then incubated at 30 °C for 30 min with gentle agitation. The denaturation buffer was added and the mixture was heated at 90 °C for 5 min to complete the denaturation process. The beads were isolated with the magnet, the supernatant was loaded in 4 to 12% Bis-Tris gels. For the non-radioactive fraction, we performed western blotting as described above, in the section on “biochemical analyses”. The radioactive blot was dried onto Whatman filter paper for two hours. The dried-down gel was then placed against a phosphor screen. Two hours of incubation were sufficient for the detection of radiolabelled phosphorylated proteins. The phosphor screen was scanned with a Cyclone Plus machine (Perkin Elmer) and the number of DLU (density light unit) was determined with the software provided.

2.4. Stereotaxic injection

Adult male Sprague-Dawley rats (Charles River Laboratories) weighing ~250 g were housed under a 12 h light/12 h dark cycle, with *ad libitum* access to food and water, in accordance with European Community (Directive 2010–63/EEC) and French (Code Rural R214/87–130) regulations. Experimental procedures were approved by the local ethics committee and registered with the French Research Ministry (committee #44, approval #12–100 and APAFIS#1372-2015080415269690v2). For stereotaxic injections, the animals were deeply anaesthetised with 4% isoflurane followed by a mixture of ketamine (75 mg/kg) and xylazine (5 mg/kg), and placed in a stereotaxic frame. Recombinant lentiviruses and adeno-associated viral vectors were injected bilaterally into the substantia nigra, at the following stereotaxic co-ordinates: +3.4 mm anterior to the interaural zero and ± 2.0 mm lateral to bregma, at a depth of −7.8 mm relative to the skull, with the tooth bar set at −3.3 mm (Supplementary Fig. S1, B and F). For striatal injections of lentiviral vectors, the following coordinates were used: +0.86 mm anterior to the interaural zero and ± 4.0 mm lateral to bregma, at a depth of −4.5 mm relative to the skull, with the tooth bar set at −3.3 mm. We injected 2 μl of virus (200 ng for lentiviruses and 5×10^{10} viral particles for AAV into each site), with a 34-gauge blunt-tipped needle linked to a 10 μl Hamilton syringe by a polyethylene catheter, at a rate of 0.25 μl/min, with an automatic pump (CMA-4004). The needle was left in place for 5 min and was then slowly

withdrawn.

2.5. Behavioural analysis

The Catwalk method (Noldus information Technology, Wageningen, the Netherlands) is an automated and computerised gait-analysis technique for the objective quantification of multiple static and dynamic gait parameters. The following gait parameters were calculated: intensity of the paw print intensity, print length, print width, print area (surface area of the complete print), stand, swing (duration for which there was no contact with the glass plate in a step cycle), swing speed (speed of the paw during swing), stand index, stride length (the distance between successive placements of the same paw), and angle. All rats were trained to cross the runway in a consistent manner, during at least three training sessions per day, before the experiment was begun. Analysis was performed on a minimum of three normal step sequence patterns in each uninterrupted run.

2.6. Tissue processing

For all procedures, rats were first deeply anaesthetised by isoflurane inhalation followed by the intraperitoneal injection of a lethal dose of sodium pentobarbital.

For immunohistochemistry, rats were transcardially perfused with 300 ml of 4% paraformaldehyde in phosphate buffer at a rate of 30 ml/min. After perfusion, the brain of each rat was removed quickly and immersed in ice-cold 4% paraformaldehyde for at least 24 h, before transfer to 15% sucrose for 24 h and then 30% sucrose the next day, for cryoprotection. The brains were then cut into 40 µm sections on a freezing microtome (CM1900, Leica, Germany). Serial sections of the striatum and midbrain were stored in antifreeze solution (30% sucrose, 30% ethylene glycol in PBS) until use.

2.7. Immunohistological analysis and quantification

2.7.1. Immunohistochemistry

The sections were removed from the antifreeze solution and washed in PBS. Endogenous peroxidase activity was quashed by transferring these sections to 1% H_2O_2 for 30 min at room temperature (RT) and washing them three times with PBS, for 10 min each. The sections were then blocked by incubation with 4.5% normal goat serum for 30 min in PBS-T (0.2% Triton X-100 in PBS) and they were then incubated overnight with primary antibody in 3% normal goat serum in PBS-T, at 4 °C, with gentle shaking (anti-tyrosine hydroxylase (TH) antibody: MAB318 clone LNC1, 1:3000; anti-hemagglutinin tag (HA), Covance clone 11, 1:1000). The next day, these sections were removed from the primary antibody solution, washed three times and incubated for 1 h at room temperature with the appropriate biotinylated secondary antibody in PBS-T (Vector Laboratories, Burlingame, CA, USA, 1:1000). The sections were then washed and incubated with ABC complex solution in PBS-T (1:250, reagents A and B combined in a 1:1 ratio, Vector Laboratories) for 1 h. The sections were then incubated with DAB for 30 s to 1 min and mounted on slides, in Eukitt mounting medium.

2.7.2. Cell counting

Optical fractionators sampling was carried out on a Zeiss microscope AxioPlan. Midbrain dopaminergic neurons were outlined on the basis of TH immunolabelling, with reference to a coronal atlas of the rat brain (Paxinos and Watson, 6th edition). For the lentiviral-mediated transduction of DA neurons, TH-positive cells in vicinity of the injection site were counted and the number of positive neurons per section was calculated with Mercator Software (Explora Nova, France). We placed 100 × 100 µm grids in a systematic random manner, 80 × 80 µm apart, with a 3 µm offset from the surface of the section. Quantification was performed on five serial sections spaced by 200 µm, from the anterior to the middle of the SNc, corresponding to the infection volume. For the AAV-mediated transduction of DA neurons, TH-positive cells were evaluated by unbiased stereology in the entire SNc. The same parameters were used as described above.

2.7.3. Immunofluorescence

The procedure used was similar to that for immunohistochemistry, but without the incubation in 1% H_2O_2. The primary antibodies used for the immunofluorescence procedure were directed against TH (AB152 1:1000, EMD Millipore, US) and HA (Covance clone11, 1:1000). On the first day, sections were incubated with the primary antibody against TH overnight at 4 °C. The next day, they were incubated with a fluorescent secondary antibody: Alexa Fluor 594-labelled goat anti-rabbit IgG (1:1000, Life Technologies) for 1 h at RT. The sections were then washed and incubated overnight at 4 °C with another primary antibody directed against HA. Finally, they were incubated with a second fluorescent secondary antibody, Alexa Fluor 488-labelled goat anti-mouse IgG (1:1000, Life Technologies) for 1 h at room temperature. The sections were stained with DAPI, washed and mounted in a fluorescence mounting medium. Images were acquired with a laser confocal microscope (SP8, Leica, Germany) or an epifluorescence microscopy (DM8000, Leica, Germany).

2.7.4. Measurement of transduction volumes after lentiviral injection in the substantia nigra

Transduction volume was evaluated by epifluorescence microscopy. Serial sections were taken from each animal: five to six sections 400 µm apart, covering the entire SNc. The SNc was segmented on the basis of TH staining, analysed in the red channel, and the area was measured. TH segmentation was analysed in the green channel, corresponding to HA staining, and the zone of positive green staining within the TH area was segmented and measured. The transduction volume was calculated from the percentage of transduction measured for each section.

2.8. Real-time quantitative PCR

The transcriptomic analysis was performed on rat striatum, to ensure that it was performed on a relatively homogeneous population of transduced neurons. Rats were infected with the different LVs coding for ΔLRRK2 and LV-GFP. The striatal region displaying fluorescence was dissected out with a circular punch (1.5 mm in diameter) from 1 mm-thick fresh coronal brain sections visualized under a fluorescence binocular microscope (Leica). The punch samples were crushed and stored in Trizol solution (Life Technologies) at −80 °C before processing. Total RNA was treated with DNase RQ1 and reverse-transcribed with the SuperScript™ III reverse transcriptase (VILO kit, Life Technologies). The rat Huntington's disease RT^2 profiler PCR array (Qiagen) was used to evaluate gene expression directly and to assess potential involvement in striatal disease. cDNAs were generated in accordance with the array manufacturer's instructions. The list of the 88 mRNA analysed can be found at https://www.qiagen.com/be/shop/genes-and-pathways/complete-biology-list/huntingtons-disease/. A statistical analysis was performed to identify genes upregulated or downregulated in the GS group relative to the WT or dead kinase (DK) group. The expression of the genes identified with the RT^2 profiler PCR array were checked in SYBR Green-based real-time quantitative RT-PCR assays performed in triplicate with the *Taq* Platinum enzyme (SYBR Green qPCR kit, Invitrogen) on a Master cycler Realplex system (Eppendorf) with different primers designed and validated in house (Supplementary Table 1).

2.9. Statistical analysis

Data were analysed by two-tailed, one-way analysis of variance (ANOVA) performed with Statistica software (Statsoft Inc., Tulsa, Oklahoma, USA) and, when appropriate, Bonferroni *post hoc* correction for multiple comparisons was applied. Unpaired Student's *t*-tests were

performed for pairwise comparisons. For the analysis of gene array, results (n = 6/group) showed that data distribution was not normal so that non-parametric tests were used. When Kruskal-Wallis test showed significance, Mann-Whitney *post hoc* test was applied for comparison between groups. The annotations used to indicate the level of significance are as follows: *$p < .05$; **$p < .01$; ***$p < .001$.

3. Results

3.1.1. Functional and biochemical characterization of ΔLRRK2

The expression of the different fragments was first evaluated *in vitro* after the transfection of HEK293T cells with expression vectors encoding the K, RCK or RCKWD40 (ΔLRRK2) [1326–2527 a.a.] fragments of LRRK2, with or without the G2019S mutation (Fig. 1A). We added an HA tag to the C-terminus of all constructs. RT-qPCR analysis after transfection showed that mRNA coding for K, RCK and ΔLRRK2 were not expressed at statistically different levels, although the larger fragment ΔLRRK2 tended to be less expressed compared to the smaller fragments (Fig. 1B). After protein extraction in buffer with non-ionic detergents (NP40 and Triton X100), western blot analysis based on detection of the HA tag showed that the fragments migrated at their expected molecular weights: 30 kDa for K, 100 kDa for RCK and ~143 kDa for ΔLRRK2, demonstrating an absence of abnormal cleavage or instability (Fig. 1C). The detection and the quantification of protein levels were done with the HA tag. Only for the K fragment, a small but significant difference was seen between the expression of the G2019S form when compared to the WT form (Fig. 1D). RCK and RCKWD40 (ΔLRRK2) forms tended to be much less expressed than the smaller fragment K but no significant differences were seen between RCK^{WT} and RCK^{G2019S} or $\Delta LRRK2^{WT}$ and $\Delta LRRK2^{G2019S}$. To better focus on the comparison between $\Delta LRRK2^{WT}$ and $\Delta LRRK2^{G2019S}$, we repeated the transfection experiment, protein extraction and quantification of western blot for this long fragment (Fig. 1E). No difference of expression was detected between $\Delta LRRK2^{WT}$ and $\Delta LRRK2^{G2019S}$ (Fig. 1F).

We next asked whether the kinase activity of ΔLRRK2 could be detected. For this purpose a kinase activity assay with ^{32}P-γ-ATP in the presence of the pan-kinase substrate myelin basic protein (MBP) was performed (Galvan et al., 2018). The higher level of kinase activity observed with $LRRK2^{G2019S}$ compared to wild-type LRRK2 is thought to be a key molecular aspect of its neurotoxicity (Lee et al., 2010; West et al., 2007). This increase in kinase activity is dependent on adjacent functional domains: the presence of the ROC domain facilitates LRRK2 kinase activity and synergistically enhances G2019S-induced kinase activity (Lewis et al., 2007; Smith et al., 2006; Webber et al., 2011). For these reasons, we assessed the biochemical activity of ΔLRRK2 in comparison with two other "shorter" fragments containing the kinase domain. The three recombinant fragments containing the G2019S substitution (kinase, K^{G2019S}; ROC-COR-kinase, RCK^{G2019S}; RCK-$WD40^{G2019S}$ *i.e.* $\Delta LRRK2^{G2019S}$) were purified by HA-mediated immunoprecipitation after the transfection of HEK cells. In this radioactive assay with ^{32}P-γ-ATP, the radioactivity of the different kinase fragments was assessed after immunoprecipitation and separation by SDS-PAGE. Only $\Delta LRRK2^{G2019S}$ displayed detectable autophosphorylation similar to that reported in previous studies for the (1326–2527 aa) ΔLRRK2 (Shogo Kamikawaji et al., 2016). The K^{G2019S} and RCK^{G2019S} fragments displayed no detectable autophosphorylation in our assay. An analysis of ^{32}P incorporation into the MBP substrate was performed to determine the phosphorylation activity of the different fragments. In parallel, the levels of immune-precipitated recombinant fragments were evaluated by western blotting with an antibody directed against the HA tag (see Fig. 2, non-radioactive fraction). K^{G2019S} and RCK^{G2019S} had similar low levels of kinase activity (Fig. 2A–C). Conversely, $\Delta LRRK2^{G2019S}$ had much higher level of phosphorylation activity than the smaller fragments. We then compared the catalytic activity of $\Delta LRRK2^{G2019S}$ with that of the corresponding wild-type form, $\Delta LRRK2^{WT}$. MBP phosphorylation levels were higher with $\Delta LRRK2^{G2019S}$ than with $\Delta LRRK2^{WT}$, suggesting that the G2019S substitution had indeed increased the kinase activity of this long C-terminal fragment of LRRK2 (Fig. 2D–E).

We also studied RAB10 phosphorylation in presence of the different forms of ΔLRRK2 in HEK cells infected with lentivirus to produce stable cell lines or in HEK transfected with the full length LRRK2. Results were congruent with the literature. Only the overexpression of full length $LRRK2^{WT}$ and $LRRK2^{G2019S}$ produced an increase in phospho-RAB10 while total levels of (non-phosphorylated) RAB10 remained unchanged (Supplementary Fig. S2A, B). In our hands, the double dead mutant $LRRK2^{DK}$ produced no increase in phospho-RAB10, but the expression levels of this double mutant was found to be always low, possibly as a result of its abolished autophosphorylation which should accelerate its

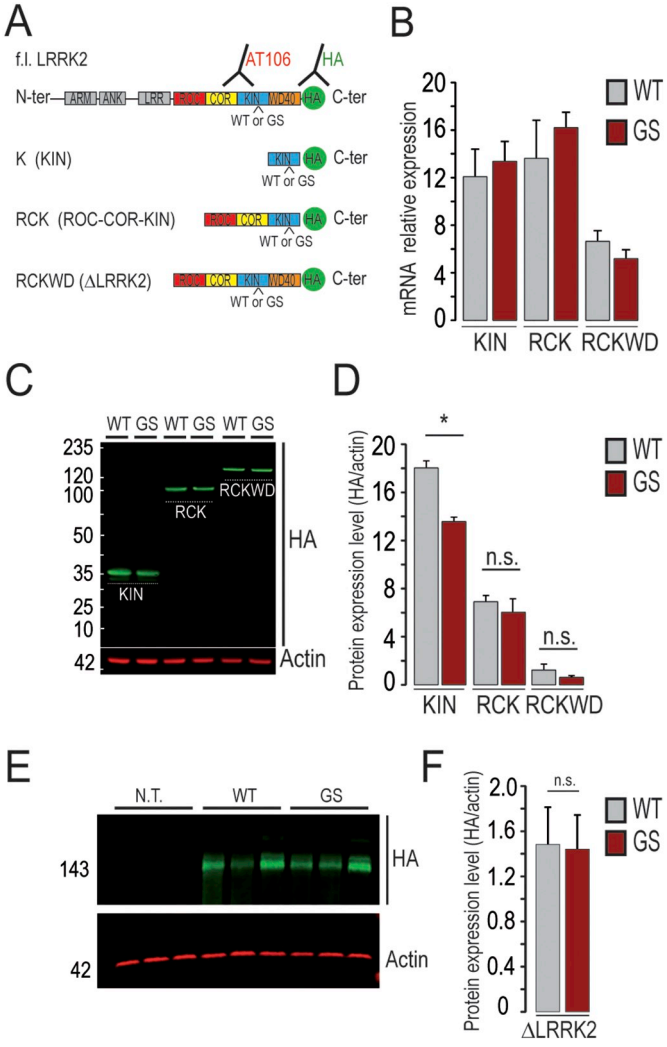

Fig. 1. Characterization of the expression of LRRK2 constructs *in vitro* in cell lines. (A) Plasmids coding for the full length (FL), kinase domain (K), the ROC/COR GTPase domain (RCK), and the RCK with the WD40 domain (RCKWD40, *i.e.* ΔLRRK2) with the addition of a hemagglutinin tag (HA) were synthetized in the WT or G2019S forms. (B) Quantitative analysis of the results from RT-qPCR on mRNA extracts after transfection of HEK293T cells with plasmids coding the different forms shown in A. (C) Western blot analysis after SDS-PAGE showed that the six different fragments migrated at their expected molecular weights when detected with the anti-HA antibody. (D) Quantification of the western blots shown in C. (E) Western blot analysis after SDS-PAGE of protein extracts obtained from three independent transfections with plasmids coding either WT or GS forms of ΔLRRK2. (F) Quantification of the western blots shown in E. *, $p < .05$; $n = 3$, Student's *t*-test for paired comparison.

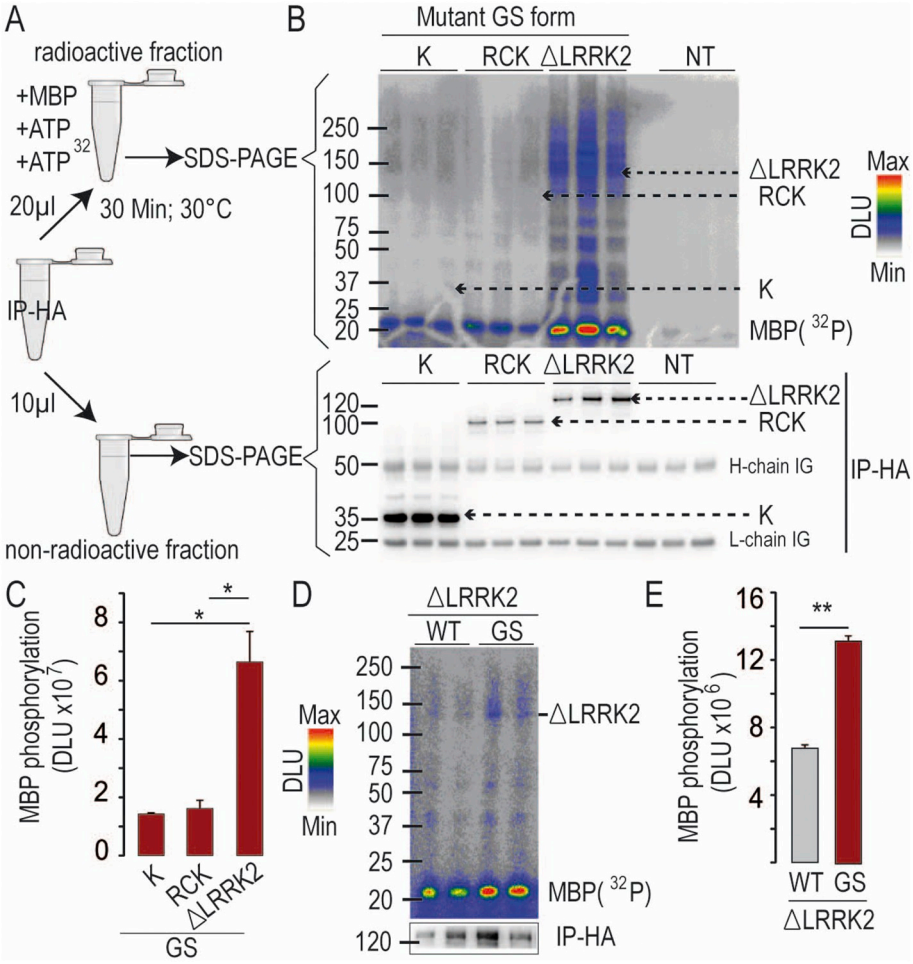

Fig. 2. Biochemical characterization of the C-terminal fragments of LRRK2. Kinase assay: Fragments were purified by HA-mediated immunoprecipitation. A portion of the magnetic beads was used to study the levels of recombinant fragments by western blotting (IP-HA). The rest of the beads were incubated with radioactive ^{32}P-ATP and myelin basic protein (MBP) as a kinase substrate (A). After incubation, K (kinase domain), RCK ROC-COR-kinase) and ΔLRRK2 (ROC-COR-kinase-WD40 domain) and MBP were separated by SDS-PAGE, and ^{32}P-labelled proteins were detected with a PhosphoImager. (B) Representative image showing ^{32}P-incorporation into MBP after incubation with each of the three fragments carrying the G2019S mutation (GS). (D) ^{32}P-incorporation into MBP after incubation in the presence of wild-type (WT) ΔLRRK2, relative to incorporation in the presence of ΔLRRK2 carrying the G2019S (GS) mutation. (C, E). Quantification of ^{32}P-incorporation into MBP. *, $p < .05$; One-way ANOVA with Bonferroni *post hoc* test.**, $p < .01$, or Student's *t*-test for paired comparison.

degradation as reported for LRRK2 (Lobbestael et al., 2016). We next used RAB10 as bait in co-immunoprecipitation experiments to investigate whether full length LRRK2 could be pulled down with RAB10. Results showed that both full length LRRK2^{WT} and LRRK2^{G2019S} could be detected in the immunoprecipitate (Supplementary Fig. S2A, C).

Similar experiments using HEK cells were carried out in parallel with ΔLRRK2^{WT} and ΔLRRK2^{G2019S} to determine whether these fragments could interact with RAB10 (Supplementary Fig. S2B, D). Results showed no detectable change in RAB10 phosphorylation in presence of ΔLRRK2 fragments. ΔLRRK2 fragments were not detected in the immunoprecipitate, indicating no major interaction with RAB10 (Supplementary Fig. S2B, D).

The preliminary biochemical characterization thus suggested that ΔLRRK2 displays a kinase activity. It also indicated that the molecular "switch" induced by G2019S mutation was preserved in the ΔLRRK2 constructs, as previously reported for the LRRK2 protein (Jaleel et al., 2007). However, ΔLRRK2 fragments do not phosphorylate the substrate of full length LRRK2, RAB10, consistent with the reported importance of the serines (S910 and S935) in the N-terminus of LRRK2 for its interaction with RAB10 and other RAB proteins (Liu et al., 2018; Steger et al., 2017).

3.1.2. *Transcriptomic analysis of LRRK2 fragments in vivo*

We investigated whether the overproduction of LRRK2 fragments had a biological effect in neurons *in vivo*. We used a straightforward and simple approach in order to target a homogeneous population of transduced neurons (which could not be done easily in the SNc to obtain a sufficient amount of neurons) and after resection of the transduced region perform a mRNA expression analysis. We chose the striatum, a region which does not degenerate in LRRK2^{G2019S} carriers, but is naturally enriched in LRRK2 (Brochier et al., 2008; Higashi et al., 2007). In these experiments, we aimed to assess the effect of LV-ΔLRRK2^{G2019S} relative to that of LVs encoding GFP, ΔLRRK2^{WT} and ΔLRRK2$^{G2019S/D1994A}$, the kinase-dead form of ΔLRRK2. The mutation D1994A is known to abolish kinase activity and was therefore used as a negative control for kinase activity (Smith et al., 2006). For the selective collection of transduced striatal tissue, we co-injected in rats LVs encoding ΔLRRK2 (100 ng p24/µl) with LV-GFP (50 ng p24/µl) (Supplementary Fig. S3). Six weeks later, we measured the expression levels of 84 striatal genes using a commercial RT-qPCR array (see Materials and methods) (Fig. 3). RT-qPCR was also performed to compare the mRNA levels for the three ΔLRRK2 transgenes and we found no significant difference between the three transgenes (Fig. 3A). The statistical analysis of expression profiles for the 84 genes showed that overexpression of ΔLRRK2^{G2019S} resulted in significant changes in the expression of eight genes, when compared to ΔLRRK2^{WT} and ΔLRRK2$^{G2019S/D1994A}$ (Fig. 3C–E). This suggested that an increase in kinase activity was required for this effect in neurons *in vivo*. The changes in expression for these genes were confirmed with a different RT-qPCR method (data not shown, primers used for RT-qPCR in Supplementary Table S1). Consistent with the lack of obvious toxicity *in vivo,* no difference was observed in the expression of genes directly related to apoptosis mechanisms (Akt, Bax, and Casp3) (Fig. 3B). ΔLRRK2^{G2019S} overexpression induced changes in mRNA levels for genes directly related to neurotransmission/cell signalling: *Tac1* (preprotachykinin/substance P), *Grin2a* (NMDA receptor subunit A), *Cnr1* (cannabinoid receptor 1), *RGS4* (regulator of G protein signalling 4) and *HPCA* (hippocalcin) were significantly downregulated in the

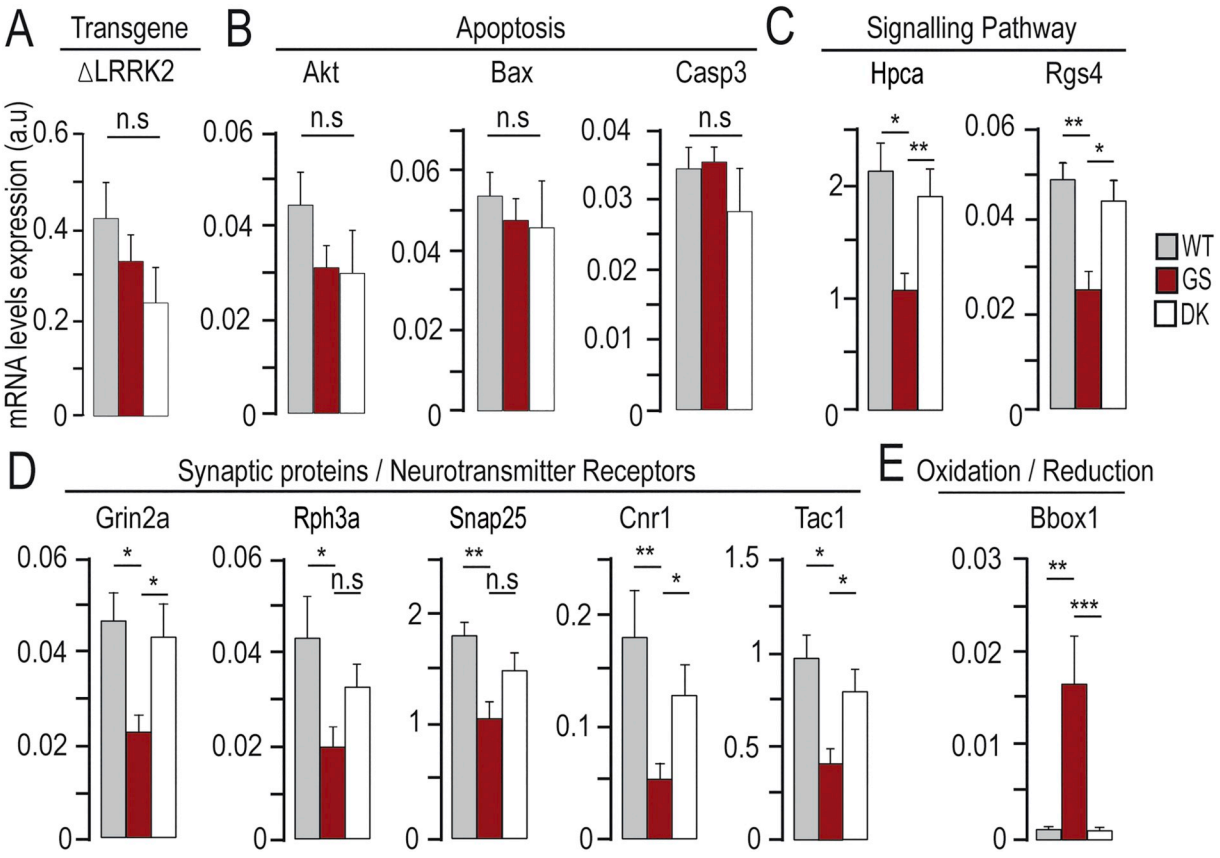

Fig. 3. Biological effects of ΔLRRK2 fragments in the striatum assessed using a RT-qPCR array. Rats received intrastriatal co-injections of LV-ΔLRRK2 [WT, G2019S or the dead kinase (DK: G2019S + D1994A) forms (100 ng/μl)] with LV-GFP (50 ng/μl) and the levels of 84 different mRNA species were measured with an RT-qPCR array at 6 weeks post-infection. (A) The levels of mRNA for each LRRK2 fragment (Transgene) were measured by RT-qPCR. (B) No major change in the expression of the apoptosis-related genes on the array was induced by $\Delta LRRK2^{G2019S}$ overexpression (Akt, Bax and Casp3). (C-E) Gene products (of the 84 on the array – see the materials and methods section) with a different level of expression in the group injected with LV-$\Delta LRRK2^{G2019S}$ than in the other groups, including (C) signalling pathway genes (HPCA, hippocalcin; RGS4, regulator of G protein signalling 4), (D) synaptic proteins and neurotransmission genes (Grin2a, NMDA receptor subunit A; Rph3a, rabphilin 3a; SNAP25, synaptosomal-associated protein 25; Cnr1, cannabinoid receptor 1; Tac1, preprotachykinin/substance P) and (E) oxidation/reduction pathway (Bbox1, gamma-butyrobetaine dioxygenase). *, $p < .05$; **, $p < .01$; ***, $p < .001$, Kruskal-Wallis, ANOVA and Mann-Whitney tests ($n = 6$/group).

$\Delta LRRK2^{G2019S}$ group relative to the other three groups (Fig. 3C-D). The levels of *Snap25* (synaptosomal-associated protein 25) and *Rph3a* (rabphilin 3a) mRNA were significantly lower following transduction with a LV encoding $\Delta LRRK2^{G2019S}$ than after transduction with LVs encoding the WT and dead-kinase forms of the ΔLRRK2 fragment (Fig. 3D). For one gene, encoding *Bbox1* (gamma-butyrobetaine dioxygenase, the enzyme responsible for L-carnitine synthesis) mRNA levels in the $\Delta LRRK2^{G2019S}$ group were more than three times those in the other groups (Fig. 3E). These results therefore indicate that overexpression of $\Delta LRRK2^{G2019S}$ can produce perturbations in neurons *in vivo*.

3.1.3. Characterization of LVs-induced transduction in the rat substantia nigra

LVs with the VSV-G envelope and coding for proteins under the control of PGK promoter are known to almost exclusively express transgenes in neuronal cells in the brain (Francelle et al., 2015; Galvan et al., 2018). We checked with LV-GFP that it was also the case in the SNc in rats. Double immunofluorescence studies showed no expression in astrocytes or microglial cells (Supplementary Fig. S4). At low magnification, after infection with LV-ΔLRRK2, the HA tag was detected in a large proportion of cells reminiscent of neurons in the SNc (Fig. 4A). Confocal analysis showed that, close to the injection site, about 90% of TH–positive (DA) neurons labelled with an antibody directed against tyrosine hydroxylase (TH) were transduced and displayed strong HA-positive immunofluorescence signal in the cytoplasm and dendrites (Fig. 4B). The pattern and intensity of fluorescence were similar for both ΔLRRK2 forms (Fig. 4A, B). As for LV-GFP, transduction of cell types other than neurons has never been observed with LV-ΔLRRK2. Quantification of the volume of SNc transduced after infection with the different LVs coding for ΔLRRK2 showed that approximately 30% of the SNc was transduced (mostly its anterior part) and no significant differences were seen between LV-$\Delta LRRK2^{G2019S}$ and LV-$\Delta LRRK2^{WT}$ (Fig. 5A–D).

3.1.4. In vivo experiments with LVs to study the potential toxic effects of LRRK2 fragments

We evaluated the potential toxicity of LV-$\Delta LRRK2^{WT}$ or LV-$\Delta LRRK2^{G2019S}$. LVs were injected into the SNc of WT rats (200 ng per site). We injected LVs encoding the WT form of ΔLRRK2 into the left hemisphere, and LVs encoding the G2019S form, which we thought might be toxic, into the right hemisphere. In addition, a control group received injections of vehicle (PBS/BSA) and a LV encoding GFP. Pilot experiments with lentiviral vector and AAVs (not shown) indicated no obvious degeneration in the SNC and no behavioural (motor) abnormalities at 10 and 15 weeks post-infection respectively. We reasoned that degeneration could occur very progressively, so we chose a 25 weeks (6 months) time point. Rats were subjected to the Catwalk® test 25 weeks after injection, for the detection of motor deficits and three days later, the rats were euthanized for histological evaluation.

We hypothesized that asymmetric abnormalities would be detected when the animals were crossing the elevated board, if the fragments

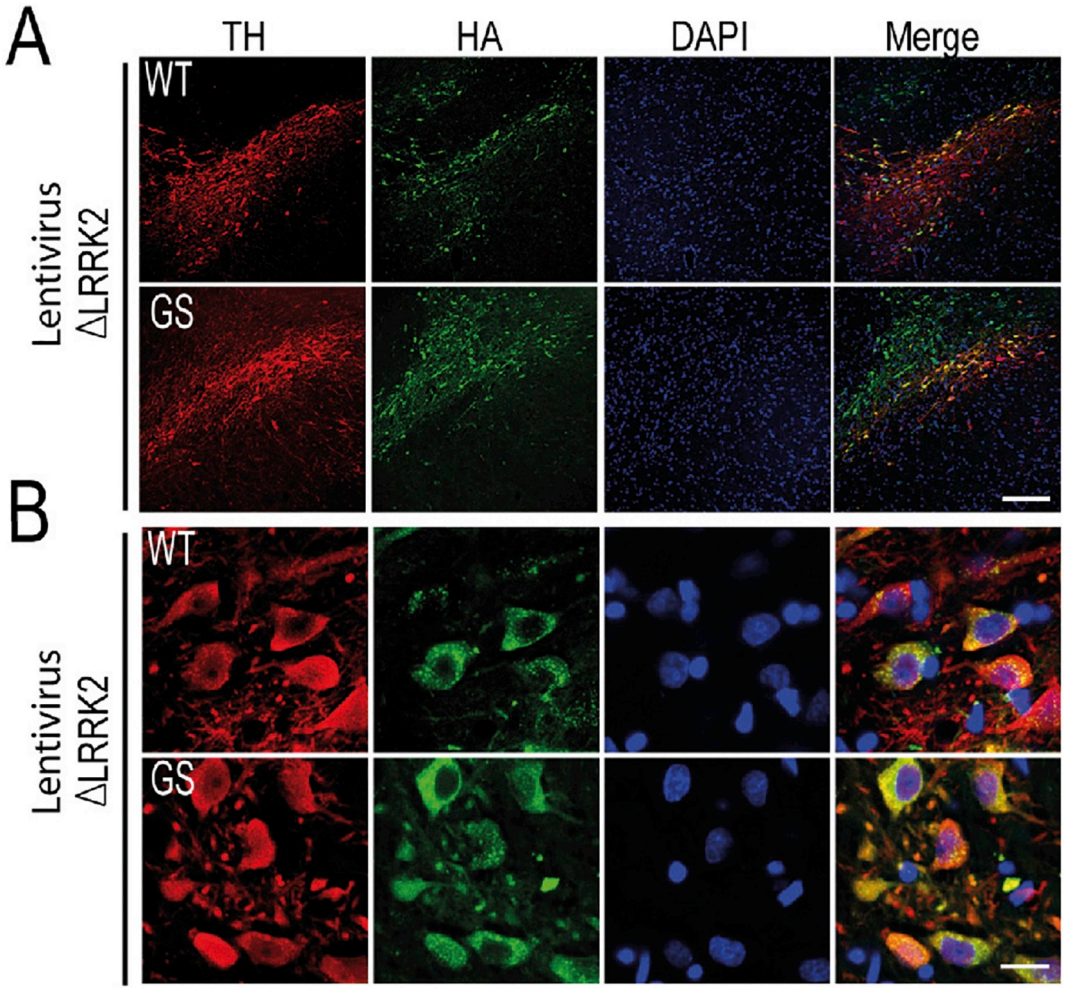

Fig. 4. Expression of ΔLRRK2 fragments at the cellular level ten weeks after infection of the SNc with AAV-ΔLRRK2. Double-immunofluorescence labelling and confocal microscopy were used to study ΔLRRK2-HA expression in transduced SNc at 10 weeks post-infection with AAV2/9-ΔLRRK2^{WT} or AAV2/9-ΔLRRK2^{G2019S} (HA-positive, green). Representative images at low (A) or high (B) magnification are shown. Note that dopaminergic cells (TH-positive, red) in SNc co-localize with ΔLRRK2 (HA-positive/TH-positive, green) (B). Scale bars in A and B: 400 μm and 10 μm respectively. (For interpretation of the references to colour in this figure legend, the reader is referred to the web version of this article.)

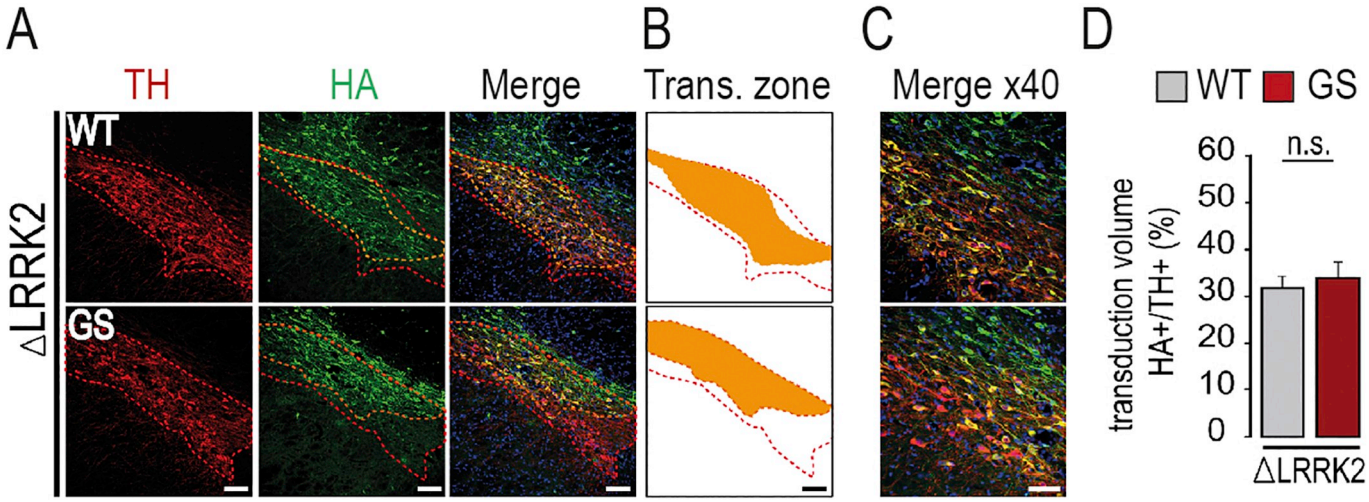

Fig. 5. Quantification of the expression of ΔLRRK2 in the SNc ten weeks after LV injection. (A) Double-immunofluorescence labelling and confocal microscopy were used to determine the volume of the SNc (TH-positive, red) at 10 weeks post infection with LV-ΔLRRK2^{WT} or LV-ΔLRRK2^{G2019S} (HA-positive, green). The TH-positive (in red) and HA-positive (in green) zones were delineated and mapped onto the merged acquisition for delimitation of the co-infected area (HA-positive/TH-positive) (B). (C) Higher magnification showing SNc neurons co-expressing TH and LRRK2 fragments. (D) Quantification was performed along the rostro-caudal extension of the total SNc to calculate, using the Cavalieri method, the volume of transduction with regard to the volume of the SNc. n = 6–7/group; unpaired Student's t-test; n.s.: non-significant. Scale bars: 200 μm. (For interpretation of the references to colour in this figure legend, the reader is referred to the web version of this article.)

harbouring the G2019S substitution resulted in a dysfunction of DA neurons after LV infection. We evaluated nine different gait parameters (Supplementary Fig. S5), including maximal contact area, mean stride length and mean swing speed, which have been reported to be altered in rat models of motor deficits (Vandeputte et al., 2010; Zhou et al., 2015). We analysed the right limb, corresponding to the left SNc infected with LVs encoding the WT form of ΔLRRK2, and the left front limb, corresponding to the right SNc infected with LVs encoding the G2019S form, separately. No significant asymmetry was observed 25 weeks after injection, for any of the parameters studied (Supplementary Fig. S5). Overall, the nine parameters studied did not differ between the rats infected with LRRK2 fragments and the rats receiving injections of PBS/BSA and LV-GFP.

We then investigated the integrity of the nigrostriatal pathway, by counting the dopaminergic neurons, which displayed TH staining, in the injected part of the SNc (Fig. 6A and B). Low-magnification observations revealed no marked loss of TH-positive cells, even in the vicinity of the injection site (Fig. 6A). As mentioned above, only a fraction (~30% on average) of the SNc cells was transduced, and these cells were close to the injection site, due to the limited diffusion of LVs. Thus, we assumed that the total loss would be limited (20–30% at most) and "diluted", making it difficult or impossible to detect this loss by determining the total number of TH-positive cells in the entire rostro-caudal extension of the SNc. We therefore counted TH-positive cells close to the injection site (−4.0 to −4.8 mm rostro-caudal from bregma) and determined relative densities. The apparent density of TH-positive cells in this part of the SNc did not differ significantly between wild-type and G2019S ΔLRRK2, or between these fragments and the control (GFP) (Fig. 6B). In conclusion, no significant differences were observed between the groups expressing $\Delta LRRK2^{WT}$ and $\Delta LRRK2^{G2019S}$.

3.1.5. Comparison between AAVs and lentiviral transduction

We hypothesized that the lack of neurotoxicity observed with lentiviral-mediated transduction of DA neurons could be due to the low level of transgene expression in comparison with what could be observed with AAVs. We compared the transduction efficacy of lentiviruses and AAVs encoding for the GFP protein at 1 month after stereotaxic injection. Results showed that the transduction by AAVs was higher than that obtained with LVs by approximately 10 fold (Fig. 7A, B). Moreover, the transduction of cells by the AAV2/9-GFP was continuous throughout the SNc, which was not the case for the LV-GFP (Fig. 7C).

As described for the LVs experiments, we carried out immunofluorescence analyses after infection with AAV-GFP to assess the transduction of neurons in the SNc as compared to other cell types. Results showed that GFP expression was almost exclusively seen in neurons (Supplementary Fig. S4).

3.1.6. Characterization of AAVs-induced transduction in the rat substantia nigra

Next, AAV2/9 vectors encoding either $\Delta LRRK2^{WT}$ or $\Delta LRRK2^{G2019S}$ under the PGK promoter and with a HA tag were injected into the SNc of adult rats. AAV preparations (batches) were diluted to similar concentrations (5×10^{10} viral particles/μl) and 2 μl of the final preparation was injected to determine the distribution of the wild-type and mutant ΔLRRK2 fragments in the SNc. Histological evaluations showed that all transduced cells expressing ΔLRRK2 (WT or G2019S) had a neuronal phenotype. Apart from neurons, no other transduced cell types were observed. Immunofluorescence detected by confocal microscopy of the HA tag was localized in the cytoplasm, with some punctate structures at 10 weeks P·I. (Fig. 8A, B). Using immunohistochemical detection of ΔLRRK2-HA and bright field microscopy, the neuronal staining appeared mainly diffuse in the cytoplasm without major punctate staining and dendrites could also be observed (Fig. 9A–P). Similar levels of expression were observed between AAV-$\Delta LRRK2^{WT}$ and AAV-$\Delta LRRK2^{G2019S}$.

3.1.7. In vivo experiments with AAVs, to study the potential toxic effects of $\Delta LRRK2^{G2019S}$

We evaluated the potential toxicity of AAV-$\Delta LRRK2^{WT}$ or AAV-$\Delta LRRK2^{G2019S}$ to dopaminergic neurons *in vivo* after their injection into the SNc. In this case, AAVs were injected bilaterally into the SNc. A control group received injections of vehicle (PBS pluronic acid). We evaluated nine different gait parameters in the CatWalk test. No significant changes were observed 25 weeks after injection, for any of the parameters studied. Overall, the nine parameters studied did not differ between the rats infected with LRRK2 fragments and the rats who received injections of vehicle (Supplementary Fig. S6). Rats were also subjected to the open field test to evaluate the spontaneous locomotion activity. No significant motor alteration was detected in this test (data not shown).

We then investigated the integrity of the nigrostriatal pathway, by counting the dopaminergic neurons, which displayed TH staining, in the SNc (Fig. 10A). In the case of AAVs, because of their good diffusion in the entire SNc, we counted TH-positive cells by unbiased stereology. The number of TH-positive cells, 25 weeks after infection, differed significantly between rats infected with AAV-$\Delta LRRK2^{WT}$ and AAV-$\Delta LRRK2^{G2019S}$ (Fig. 10A). The number of neurons was similar between

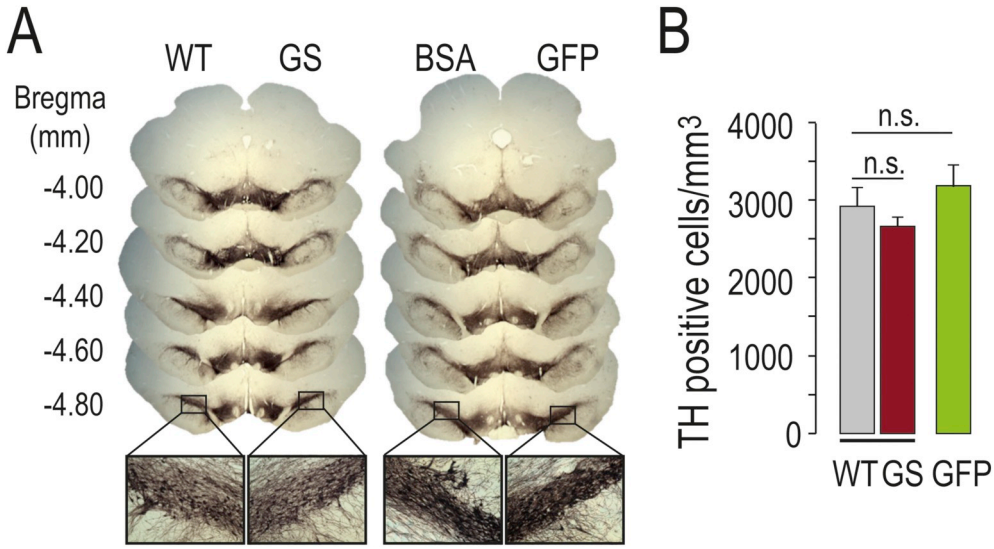

Fig. 6. Histological evaluation of the effects of wild-type and G2019S LV-ΔLRRK2 in the SNc, 25 weeks after injection. Lentiviral vectors encoding the ΔLRRK2 fragment or GFP as a control were injected into the SNc. (A) Representative histological sections of the SNc at different antero-posterior levels after immunohistochemical staining of tyrosine hydroxylase (TH). Note that TH immunohistochemistry indicates an absence of major toxicity for ΔLRRK2 in the SNc even when observed at higher magnification (bottom images). (B) The number of TH-positive neurons was counted in the part of the SNc into which the injections were made. Two-way ANOVA was used for between-group comparison; $n = 5$/group.

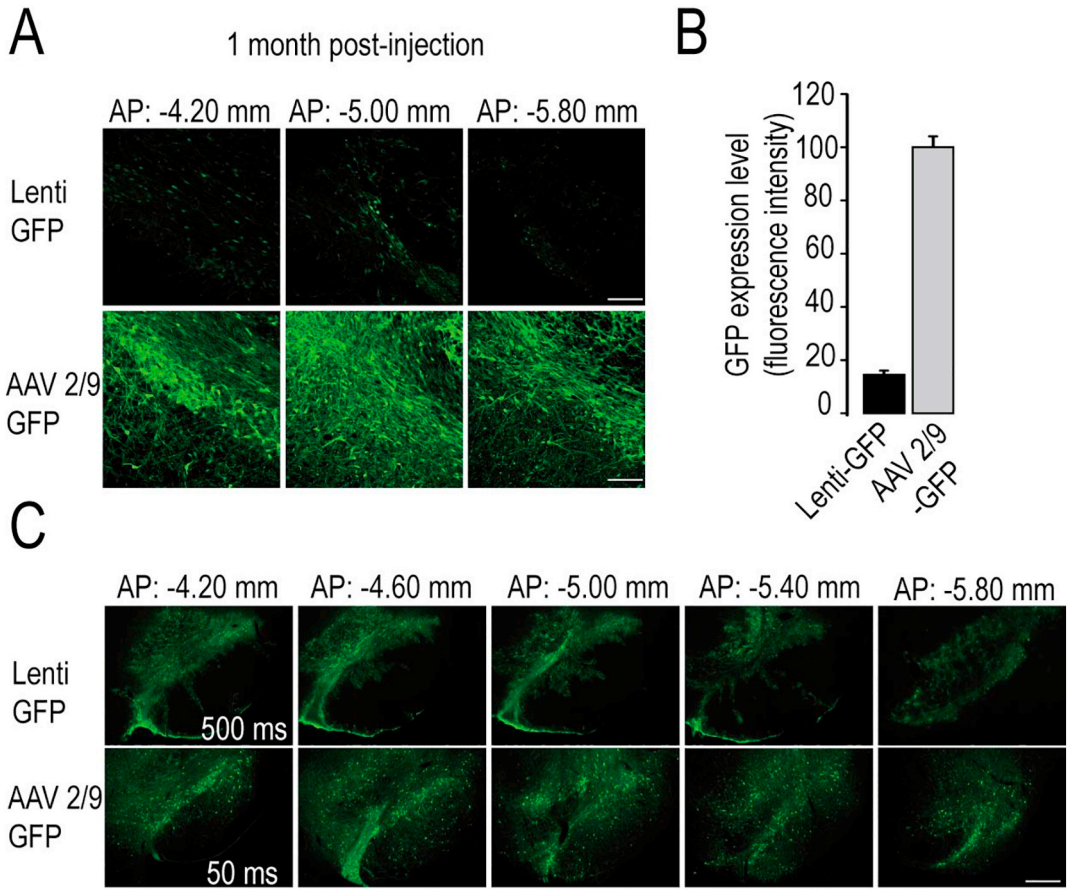

Fig. 7. Comparison between AAV and lentiviral transduction. (A) Direct GFP expression was evaluated by confocal microscopy one month post-injection of LVs or AAVs coding for the GFP protein. Acquisitions were made in three different levels of the SNc with the same confocal parameters between LV and AAV. Scale bar: 400 µm. (B) The quantification represents the mean fluorescence intensity. (C) Direct GFP expression was also evaluated by epifluorescence microscopy at low magnification. Note that for the same apparent fluorescence intensity, the time of illumination was 10 fold higher for LV-mediated transduction in comparison with AAV. n = 6 animal/group. AP: antero-posterior from Bregma. Unpaired Student's *t*-test for comparison; n.s.: non-significant. Scale bar: 500 µm.

the PBS group and the ΔLRRK2^{WT} with approximately 10,000 neurons counted. We observed a 30% decrease of TH positive neurons in the group injected with ΔLRRK2^{G2019S} as compared to the two others groups. Since apparent TH loss could be linked to a selective down regulation of the protein, we also counted by stereology the number of cells positive for the vesicular monoamine transporter (VMAT). A statistically significant loss of VMAT positive cells was also found (Fig. 10B).

In conclusion, neuronal overexpression of ΔLRRK2 with the G2019S missense mutation but not its WT form induced neurodegeneration of the nigro-striatal pathway six months after the injection of the AAVs.

4. Discussion

The toxicity of the mutant LRRK2 is thought to be related to an increase in the activity of its kinase domain. This hypothesis is particularly well supported for the G2019S substitution. In this study, we used lentiviral and adeno-associated viral vectors to express the C-terminal part of LRRK2 harbouring the G2019S mutation in the DA neurons of the rat SNc. Biochemical experiments demonstrated that the largest fragment with the G2019S substitution studied here (ΔLRRK2^{G2019S}) was "biochemically" active *in vitro* and induced changes in cells when overproduced *in vivo* in neurons. While quantitative histological studies indicated that the overexpression of ΔLRRK2^{G2019S} *via* LVs did not result in a loss of TH-positive DA neurons, results with AAVs showed that ΔLRRK2^{G2019S} induced a 30% loss of DA neurons.

A biochemical comparison of the three different types of C-terminal fragments of LRRK2 performed before the insertion of these fragments into lentiviral vectors showed that K (the kinase domain only) and RCK (the kinase domain and the ROC-COR domain) harbouring the G2019S substitution had relatively low levels of phosphorylation activity, at least in our experimental conditions *in vitro*. ΔLRRK2^{WT}, the largest fragment, containing the kinase, ROC-COR and WD40 domains, had relatively high levels of phosphorylation activity, which was significantly increased by the presence of the G2019S substitution. The higher kinase activity of the ΔLRRK2 fragment than of the shorter fragments is consistent with the previous demonstration of a requirement of the ROC-COR domain for the G2019S mutation to cause an increase in the kinase activity of the full-length LRRK2 (Jaleel et al., 2007) and the amplification of this effect by the WD40 domain (Jorgensen et al., 2009). An intramolecular mechanism involving the GTPase domain seems to play a key role in regulating the catalytic activity of LRRK2 (Taymans et al., 2011; Xiong et al., 2010).

Our biochemical analyses to investigate whether ΔLRRK2^{G2019S} could phosphorylate the LRRK2 substrate RAB10 showed, in agreement with previous studies, that the N-terminus part of LRRK2 is required for the physical interaction between the two proteins. Even when the N-terminal part of LRRK2 is partly modified by simple amino acid substitution to block phosphorylation of S910 and S935, the binding to RAB10 is disrupted and the kinase is no longer able to phosphorylate RAB10 (Steger et al., 2017). As further discussed below, ΔLRRK2 (WT or G2019S forms) is not expected to behave as the full length protein.

We then investigated whether the ΔLRRK2^{G2019S} fragment could

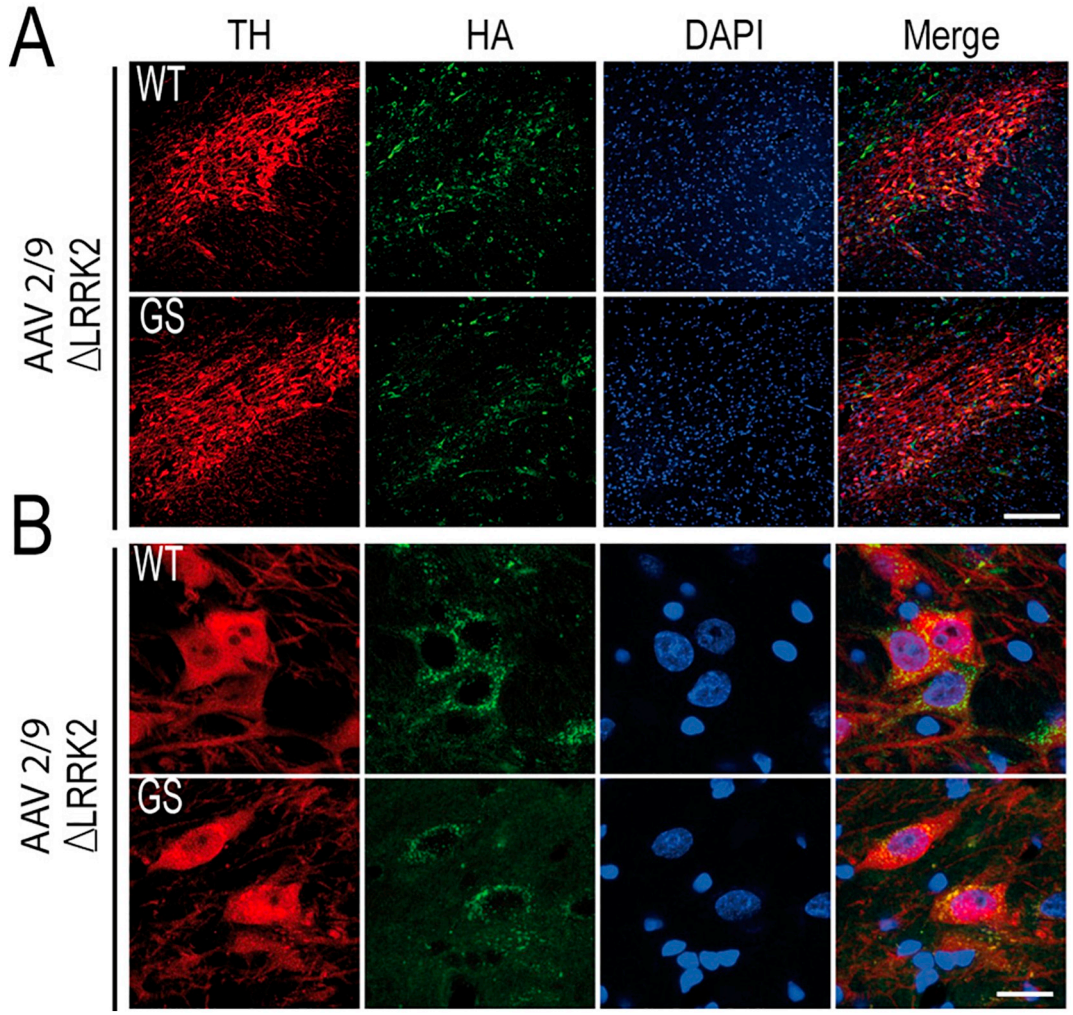

Fig. 8. Immunofluorescence analysis of *in vivo* expression of ΔLRRK2 ten weeks after infection with AAV2/9 in the SNc. (A) Double-immunofluorescence labelling and confocal microscopy were used to evaluate the specificity of AAV-ΔLRRK2^{WT} and AAV-ΔLRRK2^{G2019S} for DA neurons in the SNc at 10 weeks P.I.. (B) Higher magnification showing SNc neurons co-expressing TH and ΔLRRK2 fragments. Note that the expression of the HA tag in the SNc is not markedly different in the presence of the G2019S substitution and in the presence of the wild-type (WT) form. Scale bar: 400 μm in A and 10 μm in B.

induce a biological effect when expressed in neurons *in vivo*. Before assessing the potential toxic effects produced by ΔLRRK2^{G2019S} in the SNc neurons, a phenomenon that we assumed to require several months to be detected, we used a simple RT-qPCR array to determine whether ΔLRRK2^{G2019S} modified gene expression in neurons *in vivo* within a couple of weeks. This experiment was performed in the striatum since almost every neuron can be transduced around the site of injection in this brain region as previously shown (Francelle et al., 2015; Galvan et al., 2018), which would have been very difficult to achieve in the SNc. We found that ΔLRRK2^{G2019S} significantly modified the expression of neuronal genes with respect to the pattern of expression observed with the WT form and the catalytically inactive fragment ΔLRRK2$^{G2019S/D1994A}$. In contrast, the effects of ΔLRRK2^{G2019S} were observed in the absence of hallmarks of neurodegeneration (no changes in caspase, Bim and Bcl2 mRNA levels, and no obvious cell loss). The genes with expression patterns modified by ΔLRRK2^{G2019S} (and not ΔLRRK2$^{G2019S/D1994A}$) were all related to signalling/exocytosis and synaptic transmission. The ΔLRRK2^{G2019S}-induced reduction of neuronal genes – such as the SNAP25 gene coding for a synaptic protein and TAC1 which encodes preprotachykinin the precursor of Substance P – suggests that the LRRK2 mutation may induce an early alteration of the expression of genes related to synaptic functions in a kinase-dependent manner. Interestingly, a reduction in SNAP25 has been also reported in the brain of Lemurs infected with CAV2 to overexpress full length LRRK2^{G2019S} (Mestre-Francés et al., 2018). Reduced levels of Substance P have been reported in the SNc and in the putamen in the brains of PD patients who had not received L-DOPA therapy (Tenovuo et al., 1984). The changes in gene expression we observed are intriguing and their precise consequences remain to be determined. This finding is consistent with the key role played by LRRK2 in the regulation of synaptic mechanisms (Parisiadou et al., 2014; Piccoli et al., 2011).

At the time point considered for behavioural and histological evaluation (25 weeks after infection), rats overexpressing ΔLRRK2^{G2019S} by LVs, displayed no major signs of neurotoxicity in the dopaminergic pathway *in vivo*. Counts of DA neurons in the SNc revealed no tendency towards neuronal loss in rats expressing ΔLRRK2^{G2019S}. In contrast, rats overexpressing ΔLRRK2^{G2019S} through the injection of an AAV vector displayed a 30% neuronal loss as seen using not only TH immunochemistry but also immunochemistry of the dopaminergic marker VMAT, the vesicular transporter. We showed that at one month post-injection the protein expression level induced by AAVs was approximately 10 fold higher than that induced by LVs. These results suggested that in addition to the mutation, the level of ΔLRRK2^{G2019S} expression in the few weeks after injection was crucial to trigger a toxic effect. However, ΔLRRK2^{WT} did not produce toxicity, indicating that the G2019S-induced molecular change in the kinase domain (possibly related to an increase in the activity of its kinase) and not only a higher level of expression is required to trigger neurodegeneration in DA

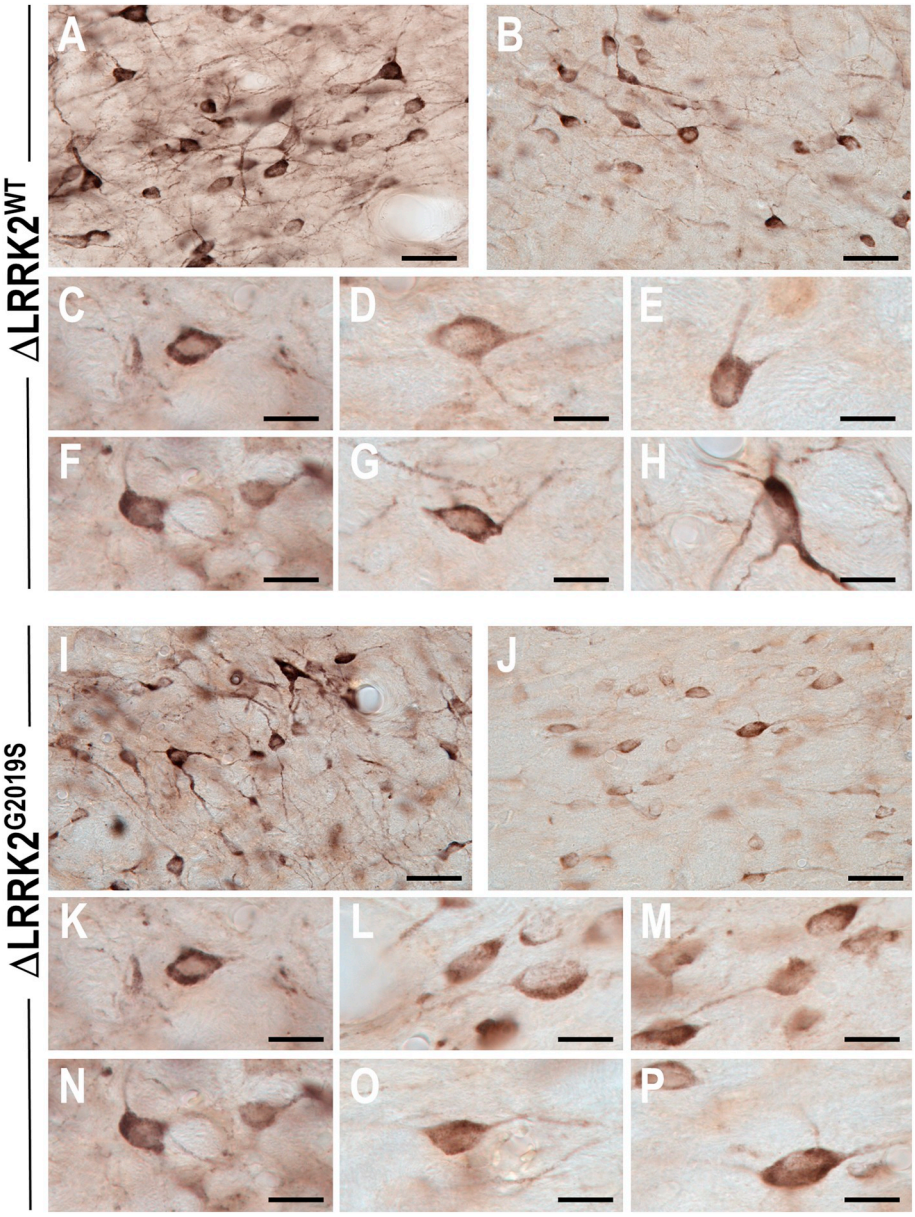

Fig. 9. Immunohistochemical analysis of the expression of ΔLRRK2 twenty five weeks after infection with AAV2/9 in the rat SNc. Photomicrographs of neurons labelled by HA-tagged ΔLRRK2 immunohistochemistry at 25 weeks post-infection in rats injected with either AAV-ΔLRRK2^{WT} (A-H) or AAV-ΔLRRK2^{G2019S} (I—P). Exposition time was set to allow light to go through labelled neurons in order to detect the potential presence of punctuate staining. Some neurons show moderate (A, I) to weak (B, J) staining. Note that the staining is relatively diffuse throughout the cytoplasm. Scale bar: 50 μm in A, B, I, J. and 10 μm in other fields of view.

neurons.

However, whereas it is probable that cell perturbations in DA neurons after expression of ΔLRRK2^{G2019S} may induce a kind of dysfunction, it did not lead to manifest motor dysfunctions. In rats expressing ΔLRRK2^{G2019S}, the chronic dysfunction of a relatively low proportion of the DA neurons in the SNc (~30%) may be compensated to hide major motor deficits. The nigrostriatal pathway is very "plastic" and capable of major compensatory mechanisms. For example, PD symptoms appear when > 70% of the DA levels in the striatum are lost.

Our data are consistent with published results, including those from studies on G2019S knock-in mice where one copy of LRRK2 is expressed (Yue et al., 2015) and BAC-transgenic rats overexpressing LRRK2^{G2019S} which have approximately 8 copies of the human gene (Lee et al., 2015). In these genetic models, no major loss of dopaminergic cells and no major motor deficits were observed, even in aged animals. This lack of effect may be due to the low level of LRRK2^{G2019S} expression, close to endogenous levels, in these transgenic animals. In our experiments, the LRRK2 transgenes were much more strongly expressed after AAV transduction (about 25–50 copies per cell) (Ruiz and Déglon, 2012). Our results are, therefore, more directly comparable with those of three groups that generated viral models of LRRK2 overexpression based on the use of adeno- or herpes simplex viruses (Ad and HSV, respectively) encoding the full-length LRRK2 protein (Dusonchet et al., 2011; Lee et al., 2010; Mestre-Francés et al., 2018). In these models, LRRK2^{G2019S} overexpression led to the partial degeneration of DA neurons in the SNc. These studies used viral vectors that underwent retrograde transport (which is not the case for the LVs and AAVs vectors used here), which means that neurons were transduced along with other cells in the striatum. It remains unclear whether the DA neuron degeneration induced by LRRK2^{G2019S} in the adenovirus, HSV and CAV2 models results purely from cell-autonomous mechanisms. The medium-sized striatal GABAergic neurons, and neighbouring glial cells are probably also infected after striatal injections of adenovirus and HSV vectors. The neurodegeneration of SNc neurons in these two models may involve changes in both DA neurons and striatal cells. In our study, ΔLRRK2^{G2019S} was overexpressed only in DA neurons and we found a comparable DA neuron loss.

The LRRK2 fragments studied here are unlikely to be able to mimic all aspects of the biology of the full-length LRRK2, because they cannot interact with partners of the N-terminal domain of LRRK2. Our

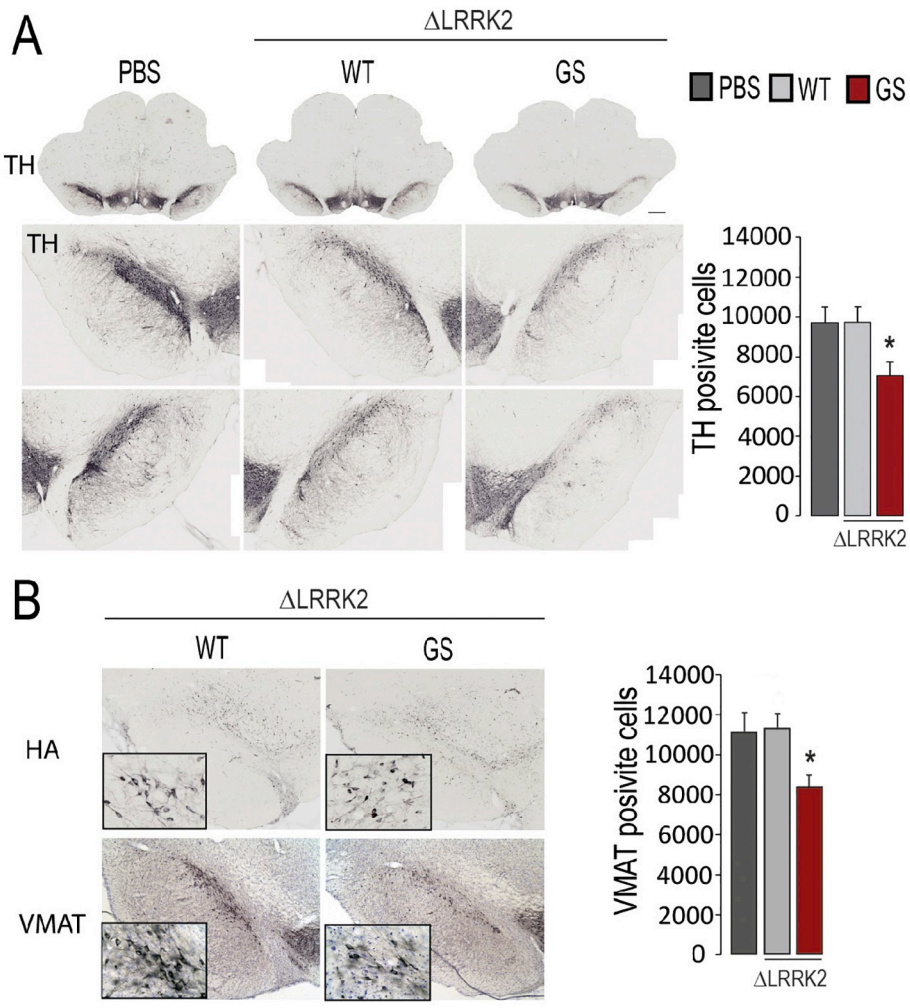

Fig. 10. Histological evaluation of the effects of wild-type and G2019S AAV-ΔLRRK2 in the SNc at 25 weeks post-injection. AAVs encoding the ΔLRRK2 fragments or PBS as a control were injected bilaterally into the SNc. (A) Tyrosine hydroxylase (TH) immunohistochemistry was performed in the SNc to evaluate the toxicity. The number of TH-positive neurons was evaluated by stereology in the entire SNc. (B) Vesicular Monoamine Transporter (VMAT2) immunochemistry was performed in the SNc and the number of VMAT-positive neurons was assessed by stereology in the entire SNc. One-way ANOVA was used for between-group comparison and Bonferroni *post hoc* correction for multiple comparisons was applied; $n = 9$/group; *, $p < .01$. Scale bar: 750 μm.

biochemical data confirmed that RAB10 is a substrate of full length LRRK2. This is coherent with recent work showing that in the SN DA neurons of both idiopathic PD patients and rat models (rotenone-based model and human α-synuclein overexpression in the SNc *via* AAV2) there is an increase of LRRK2 kinase activity. This event might lead to phosphorylation of RAB10 substrate, followed by impairment of lysosomal and mitochondrial functions (Di Maio et al., 2018). Here we showed that $\Delta LRRK2^{G2019S}$ and $\Delta LRRK2^{WT}$ cannot increase the level of phosphorylation of RAB10, underscoring that ΔLRRK2, despite its phospho-transferase catalytic activity, cannot interact with all partners of the full length LRRK2. Although RAB10 may be a key molecular player in PD, it cannot be excluded that other parallel mechanisms also contribute to mutant LRRK2-related toxicity. Substrates exist that do not require the N-terminus of LRRK2 for interaction with the kinase. Especially, the C-terminal WD40 domain is thought to be a key molecular player for the interaction of LRRK2 with different partners. For example, the WD40 domain allows LRRK2 to bind synaptic vesicles and to phosphorylate synapsin I (Marte et al., 2019; Piccoli et al., 2014). WD40 may also be involved in the interaction of LRRK2 with microtubules (Kett et al., 2012). Thus it is conceivable that $\Delta LRRK2^{G2019S}$ may trigger neurodegeneration, despite the absence of the N-terminal domain of LRRK2. ΔLRRK2 fragments provide an interesting tool for the precise evaluation *in vivo*, and more specifically in neurons, of the role of the kinase and neighbouring domains, namely the ROC-COR GTPase domain and the WD40 domain. The requirement of the ROC-COR domain for the G2019S mutation to cause an increase in the kinase activity of the full-length LRRK2 has been shown (Jaleel et al., 2007). An intramolecular mechanism involving the GTPase domain seems to play a key role in regulating the catalytic activity of LRRK2 (Taymans et al., 2011; Xiong et al., 2010). In addition, there is an amplification of this effect by the WD40 domain (Jorgensen et al., 2009). It is tempting to speculate that the differential effects between the wild type and G2019S forms of ΔLRRK2 in our experiments partly result from a change in the activity of the kinase, although this awaits further *in vivo* studies with pharmacological LRRK2 inhibitors and dead kinase mutants to be fully supported.

The ΔLRRK2 constructs are also versatile tools for studying the effects of increases in the kinase activity of $LRRK2^{G2019S}$ in different brain cells. For example, driving ΔLRRK2 expression with the GFAP promoter might be an interesting approach for studying the selective role of LRRK2's (WT and G2019S) kinase domain in astrocytes (Colin et al., 2009). These C-terminal fragments could also be used to investigate the selective role of the physiological kinase activity of LRRK2 in other types of neurons, such as striatal GABAergic neurons, in which levels of LRRK2 expression are naturally higher than in other brain regions.

LRRK2 has also been shown to interact physically or genetically with several other important proteins involved in PD. Potential "functional" interactors of LRRK2 include the α-synuclein protein (Cresto et al., 2019; Lin et al., 2009). The exact role of the kinase domain in this important interaction should be further studied. The use of truncated LRRK2 proteins such as ΔLRRK2 we used in the present study, in comparison with the full length LRRK2, could be of interest to address the existence of this functional LRRK2/α-synuclein interaction specifically in DA neurons or other cell types.

5. Conclusion

In conclusion, we present a novel molecular tool for studying the effects of the C-terminal part of LRRK2 in neurons, *in vivo*. Our results indicate that a selectively high expression in DA neurons of $\Delta LRRK2^{G2019S}$ is sufficient to induce DA neuronal loss within an experiment time frame of 6 months. These results suggest that both the expression level and the G2019S substitution-induced increase in kinase activity of the overexpressed LRRK2 fragment may be key factors to trigger cell death pathways in animal models.

Supplementary data to this article can be found online at https://doi.org/10.1016/j.nbd.2019.104614.

Declaration of Competing Interest

All authors declare that they have no conflict of interest.

Acknowledgements

This work was funded by rolling grants from the CEA and the CNRS.

The research generating these results received funding from la Fondation de France (AAP 2010-2011 and 2013, Engt 00016819). Noémie Cresto is a recipient of a PhD fellowship from Association France Parkinson (2016). The studies were also funded by European Union Horizon 2020 Programme (H2020-MSCA-ITN-2015) under the Marie Skłodowska-Curie Innovative Training Networks and Grant Agreement No. 676408.

This work benefited from a support from the national "Translational Research Infrastructure for Biotherapies in Neurosciences" (NeurATRIS, "Investissement d'Avenir", ANR-11-INBS-0011).

References

Aufschnaiter, A., Kohler, V., Walter, C., Tosal-castano, S., 2018. The enzymatic core of the Parkinson's disease-associated protein LRRK2 impairs mitochondrial biogenesis in aging yeast. Front. Mol. Neurosci. 11, 1–15.

Aurnhammer, C., Haase, M., Muether, N., Hausl, M., Rauschhuber, C., Huber, I., Nitschko, H., Busch, U., Sing, A., Ehrhardt, A., et al., 2012. Universal real-time PCR for the detection and quantification of adeno-associated virus serotype 2-derived inverted terminal repeat sequences. Hum. Gene Ther. Methods 23, 18–28.

Beccano-Kelly, D.A., Kuhlmann, N., Tatarnikov, I., Volta, M., Munsie, L.N., Chou, P., Cao, L.-P., Han, H., Tapia, L., Farrer, M.J., et al., 2014. Synaptic function is modulated by LRRK2 and glutamate release is increased in cortical neurons of G2019S LRRK2 knock-in mice. Front. Cell. Neurosci. 8.

Berger, A., Lorain, S., Joséphine, C., Desrosiers, M., Peccate, C., Voit, T., Garcia, L., Sahel, J.-A., Bemelmans, A.-P., 2015. Repair of rhodopsin mRNA by spliceosome-mediated RNA trans-splicing: a new approach for autosomal dominant retinitis pigmentosa. Mol. Ther. 23, 918–930.

Braak, H., Braak, E., 2000. Pathoanatomy of Parkinson's disease. J. Neurol. 247, II3–II10.

Brochier, C., Gaillard, M.-C., Diguet, E., Caudy, N., Dossat, C., Ségurens, B., Wincker, P., Roze, E., Caboche, J., Hantraye, P., et al., 2008. Quantitative gene expression profiling of mouse brain regions reveals differential transcripts conserved in human and affected in disease models. Physiol. Genomics 33, 170–179.

Colin, A., Faideau, M., Dufour, N., Auregan, G., Hassig, R., Andrieu, T., Brouillet, E., Hantraye, P., Bonvento, G., Déglon, N., 2009. Engineered lentiviral vector targeting astrocytes in vivo. Glia 57, 667–679.

Cookson, M.R., 2010. The role of leucine-rich repeat kinase 2 (LRRK2) in Parkinson's disease. Nat. Rev. Neurosci. 11, 791–797.

Cresto, N., Gardier, C., Gubinelli, F., Gaillard, M.-C., Liot, G., West, A.B., Brouillet, E., 2019. The unlikely partnership between LRRK2 and α-synuclein in Parkinson's disease. Eur. J. Neurosci. 49, 339–363.

Di Maio, R., Hoffman, E.K., Rocha, E.M., Keeney, M.T., Sanders, L.H., De Miranda, B.R., Zharikov, A., Van Laar, A., Stepan, A.F., Lanz, T.A., et al., 2018. LRRK2 activation in idiopathic Parkinson's disease. Sci. Transl. Med. 10, eaar5429.

Dusonchet, J., Kochubey, O., Stafa, K., Young, S.M., Zufferey, R., Moore, D.J., Schneider, B.L., Aebischer, P., 2011. A rat model of progressive nigral neurodegeneration induced by the Parkinson's disease-associated G2019S mutation in LRRK2. J. Neurosci. 31, 907–912.

Francelle, L., Galvan, L., Gaillard, M.C., Guillermier, M., Houitte, D., Bonvento, G., Petit, F., Jan, C., Dufour, N., Hantraye, P., et al., 2015. Loss of the thyroid hormone-binding protein Crym renders striatal neurons more vulnerable to mutant huntingtin in Huntington's disease. Hum. Mol. Genet. 24, 1563–1573.

Galvan, L., Francelle, L., Gaillard, M.-C., de Longprez, L., Carrillo-de Sauvage, M.-A., Liot, G., Cambon, K., Stimmer, L., Luccantoni, S., Flament, J., et al., 2018. The striatal kinase DCLK3 produces neuroprotection against mutant huntingtin. Brain 141, 1434–1454.

Gilks, W.P., Abou-Sleiman, P.M., Gandhi, S., Jain, S., Singleton, A., Lees, A.J., Shaw, K., Bhatia, K.P., Bonifati, V., Quinn, N.P., et al., 2005. A common LRRK2 mutation in idiopathic Parkinson's disease. Lancet 365, 415–416.

Healy, D.G., Falchi, M., O'Sullivan, S.S., Bonifati, V., Durr, A., Bressman, S., Brice, A., Aasly, J., Zabetian, C.P., Goldwurm, S., et al., 2008. Phenotype, genotype, and worldwide genetic penetrance of LRRK2-associated Parkinson's disease: a case-control study. Lancet Neurol. 7, 583–590.

Higashi, S., Moore, D.J., Colebrooke, R.E., Biskup, S., Dawson, V.L., Arai, H., Dawson, T.M., Emson, P.C., 2007. Expression and localization of Parkinson's disease-associated leucine-rich repeat kinase 2 in the mouse brain. J. Neurochem. 100, 368–381.

Hottinger, A.F., Azzouz, M., Déglon, N., Aebischer, P., Zurn, A.D., 2000. Complete and long-term rescue of lesioned adult motoneurons by lentiviral-mediated expression of glial cell line-derived neurotrophic factor in the facial nucleus. J. Neurosci. 20, 5587–5593.

Jaleel, M., Nichols, R.J., Deak, M., Campbell, D.G., Gillardon, F., Knebel, A., Alessi, D.R., 2007. LRRK2 phosphorylates moesin at threonine-558: characterization of how Parkinson's disease mutants affect kinase activity. Biochem. J. 405, 307–317.

Jorgensen, N.D., Peng, Y., Ho, C.C.-Y., Rideout, H.J., Petrey, D., Liu, P., Dauer, W.T., 2009. The WD40 domain is required for LRRK2 neurotoxicity. PLoS One 4.

Kamikawaji, Shogo, Ito, Genta, Iwatsubo, Takeshi, 2016. Identification of the Autophosphorylation Sites of LRRK2.

Kett, L.R., Boassa, D., Ho, C.C.-Y., Rideout, H.J., Hu, J., Terada, M., Ellisman, M., Dauer, W.T., 2012. LRRK2 Parkinson disease mutations enhance its microtubule association. Hum. Mol. Genet. 21, 890–899.

Lee, B.D., Shin, J.-H., VanKampen, J., Petrucelli, L., West, A.B., Ko, H.S., Lee, Y., Maguire-Zeiss, K.A., Bowers, W.J., Federoff, H.J., et al., 2010. Inhibitors of leucine rich repeat kinase 2 (LRRK2) protect against LRRK2-models of Parkinson's disease. Nat. Med. 16, 998–1000.

Lee, J.-W., Tapias, V., Di Maio, R., Greenamyre, J.T., Cannon, J.R., 2015. Behavioral, neurochemical, and pathologic alterations in bacterial artificial chromosome transgenic G2019S leucine-rich repeated kinase 2 rats. Neurobiol. Aging 36, 505–518.

Lesage, S., Brice, A., 2009. Parkinson's disease: from monogenic forms to genetic susceptibility factors. Hum. Mol. Genet. 18, R48–R59.

Lewis, P.A., Greggio, E., Beilina, A., Jain, S., Baker, A., Cookson, M.R., 2007. The R1441C mutation of LRRK2 disrupts GTP hydrolysis. Biochem. Biophys. Res. Commun. 357, 668–671.

Lin, X., Parisiadou, L., Gu, X.-L., Wang, L., Shim, H., Sun, L., Xie, C., Long, C.-X., Yang, W.-J., Ding, J., et al., 2009. Leucine-rich repeat kinase 2 regulates the progression of neuropathology induced by Parkinson's-disease-related mutant alpha-synuclein. Neuron 64, 807–827.

Liu, Z., Bryant, N., Kumaran, R., Beilina, A., Abeliovich, A., Cookson, M.R., West, A.B., 2018. LRRK2 phosphorylates membrane-bound Rabs and is activated by GTP-bound Rab7L1 to promote recruitment to the trans-Golgi network. Hum. Mol. Genet. 27, 385–395.

Lobbestael, E., Civiero, L., Wit, T.D., Taymans, J.-M., Greggio, E., Baekelandt, V., 2016. Pharmacological LRRK2 kinase inhibition induces LRRK2 protein destabilization and proteasomal degradation. Sci. Rep. 6, 33897.

Marte, A., Russo, I., Rebosio, C., Valente, P., Belluzzi, E., Pischedda, F., Montani, C., Lavarello, C., Petretto, A., Fedele, E., et al., 2019. Leucine-rich repeat kinase 2 phosphorylation on synapsin I regulates glutamate release at pre-synaptic sites. J. Neurochem.

Mata, I.F., Wedemeyer, W.J., Farrer, M.J., Taylor, J.P., Gallo, K.A., 2006. LRRK2 in Parkinson's disease: protein domains and functional insights. Trends Neurosci. 29, 286–293.

Mestre-Francés, N., Serratrice, N., Gennetier, A., Devau, G., Cobo, S., Trouche, S.G., Fontès, P., Zussy, C., De Deurwaerdere, P., Salinas, S., et al., 2018. Exogenous LRRK2G2019S induces parkinsonian-like pathology in a nonhuman primate. JCI Insight 3.

Naldini, L., Blömer, U., Gage, F.H., Trono, D., Verma, I.M., 1996. Efficient transfer, integration, and sustained long-term expression of the transgene in adult rat brains injected with a lentiviral vector. Proc. Natl. Acad. Sci. U. S. A. 93, 11382–11388.

Nalls, M.A., Pankratz, N., Lill, C.M., Do, C.B., Hernandez, D.G., Saad, M., DeStefano, A.L., Kara, E., Bras, J., Sharma, M., et al., 2014. Large-scale meta-analysis of genome-wide association data identifies six new risk loci for Parkinson's disease. Nat. Genet. 46, 989–993.

Paisán-Ruíz, C., Jain, S., Evans, E.W., Gilks, W.P., Simón, J., van der Brug, M., de Munain, A.L., Aparicio, S., Gil, A.M., Khan, N., et al., 2004. Cloning of the gene containing mutations that cause PARK8-linked Parkinson's disease. Neuron 44, 595–600.

Parisiadou, L., Yu, J., Sgobio, C., Xie, C., Liu, G., Sun, L., Gu, X.-L., Lin, X., Crowley, N.A., Lovinger, D., et al., 2014. LRRK2 regulates synaptogenesis and dopamine receptor activation through modulation of PKA activity. Nat. Neurosci. 17, 367–376.

Pereira, C., Miguel Martins, L., Saraiva, L., 2014. LRRK2, but not pathogenic mutants, protects against H2O 2 stress depending on mitochondrial function and endocytosis in a yeast model. Biochim. Biophys. Acta - Gen. Subj. 1840, 2025–2031.

Piccoli, G., Condliffe, S.B., Bauer, M., Giesert, F., Boldt, K., Astis, S.D., Meixner, A., Sarioglu, H., Vogt-Weisenhorn, D.M., Wurst, W., et al., 2011. LRRK2 controls synaptic vesicle storage and mobilization within the recycling pool. J. Neurosci. 31, 2225–2237.

Piccoli, G., Onofri, F., Cirnaru, M.D., Kaiser, C.J.O., Jagtap, P., Kastenmüller, A., Pischedda, F., Marte, A., von Zweydorf, F., Vogt, A., et al., 2014. Leucine-rich repeat kinase 2 binds to neuronal vesicles through protein interactions mediated by its C-terminal WD40 domain. Mol. Cell. Biol. 34, 2147–2161.

Poewe, W., 2008. Non-motor symptoms in Parkinson's disease. Eur. J. Neurol. 15, 14–20.

Ramonet, D., Daher, J.P.L., Lin, B.M., Stafa, K., Kim, J., Banerjee, R., Westerlund, M., Pletnikova, O., Glauser, L., Yang, L., et al., 2011. Dopaminergic neuronal loss,

reduced neurite complexity and autophagic abnormalities in transgenic mice expressing G2019S mutant LRRK2. PLoS One 6.
Rodriguez-Oroz, M.C., Jahanshahi, M., Krack, P., Litvan, I., Macias, R., Bezard, E., Obeso, J.A., 2009. Initial clinical manifestations of Parkinson's disease: features and pathophysiological mechanisms. Lancet Neurol. 8, 1128–1139.
Ruiz, M., Déglon, N., 2012. Viral-mediated overexpression of mutant huntingtin to model HD in various species. Neurobiol. Dis. 48, 202–211.
Satake, W., Nakabayashi, Y., Mizuta, I., Hirota, Y., Ito, C., Kubo, M., Kawaguchi, T., Tsunoda, T., Watanabe, M., Takeda, A., et al., 2009. Genome-wide association study identifies common variants at four loci as genetic risk factors for Parkinson's disease. Nat. Genet. 41, 1303–1307.
Sheng, D., Qu, D., Kwok, K.H.H., Ng, S.S., Lim, A.Y.M., Aw, S.S., Lee, C.W.H., Sung, W.K., Tan, E.K., Lufkin, T., et al., 2010. Deletion of the WD40 domain of LRRK2 in zebrafish causes parkinsonism-like loss of neurons and locomotive defect. PLoS Genet. 6.
Smith, W.W., Pei, Z., Jiang, H., Dawson, V.L., Dawson, T.M., Ross, C.A., 2006. Kinase activity of mutant LRRK2 mediates neuronal toxicity. Nat. Neurosci. 9, 1231–1233.
Steger, M., Diez, F., Dhekne, H.S., Lis, P., Nirujogi, R.S., Karayel, O., Tonelli, F., Martinez, T.N., Lorentzen, E., Pfeffer, S.R., et al., 2017. Systematic proteomic analysis of LRRK2-mediated Rab GTPase phosphorylation establishes a connection to ciliogenesis. ELife 6.
Taymans, J.-M., Vancraenenbroeck, R., Ollikainen, P., Beilina, A., Lobbestael, E., De Maeyer, M., Baekelandt, V., Cookson, M.R., 2011. LRRK2 kinase activity is dependent on LRRK2 GTP binding capacity but independent of LRRK2 GTP binding. PLoS One 6.
Tenovuo, O., Rinne, U.K., Viljanen, M.K., 1984. Substance P immunoreactivity in the post-mortem parkinsonian brain. Brain Res. 303, 113–116.
Vandeputte, C., Taymans, J.-M., Casteels, C., Coun, F., Ni, Y., Van Laere, K., Baekelandt, V., 2010. Automated quantitative gait analysis in animal models of movement disorders. BMC Neurosci. 11, 92.
Webber, P.J., Smith, A.D., Sen, S., Renfrow, M.B., Mobley, J.A., West, A.B., 2011. Autophosphorylation in the leucine-rich repeat kinase 2 (LRRK2) GTPase domain modifies kinase and GTP-binding activities. J. Mol. Biol. 412, 94–110.
West, A.B., Moore, D.J., Choi, C., Andrabi, S.A., Li, X., Dikeman, D., Biskup, S., Zhang, Z., Lim, K.-L., Dawson, V.L., et al., 2007. Parkinson's disease-associated mutations in LRRK2 link enhanced GTP-binding and kinase activities to neuronal toxicity. Hum. Mol. Genet. 16, 223–232.
Xiong, Y., Coombes, C.E., Kilaru, A., Li, X., Gitler, A.D., Bowers, W.J., Dawson, V.L., Dawson, T.M., Moore, D.J., 2010. GTPase activity plays a key role in the pathobiology of LRRK2. PLoS Genet. 6.
Xiong, Y., Neifert, S., Karuppagounder, S.S., Stankowski, J.N., Lee, B.D., Grima, J.C., Chen, G., Ko, H.S., Lee, Y., Swing, D., et al., 2017. Overexpression of Parkinson's disease-associated mutation LRRK2 G2019S in mouse forebrain induces behavioral deficits and α-synuclein pathology. ENeuro 4, 1–10.
Xiong, Y., Neifert, S., Karuppagounder, S.S., Liu, Q., Stankowski, J.N., Lee, B.D., Ko, H.S., Lee, Y., Grima, J.C., Mao, X., et al., 2018. Robust kinase- and age-dependent dopaminergic and norepinephrine neurodegeneration in LRRK2 G2019S transgenic mice. Proc. Natl. Acad. Sci. 115, 201712648.
Yue, M., Hinkle, K.M., Davies, P., Trushina, E., Fiesel, F.C., Christenson, T.A., Schroeder, A.S., Zhang, L., Bowles, E., Behrouz, B., et al., 2015. Progressive dopaminergic alterations and mitochondrial abnormalities in LRRK2 G2019S knock-in mice. Neurobiol. Dis. 78, 172–195.
Zhou, M., Zhang, W., Chang, J., Wang, J., Zheng, W., Yang, Y., Wen, P., Li, M., Xiao, H., 2015. Gait analysis in three different 6-hydroxydopamine rat models of Parkinson's disease. Neurosci. Lett. 584, 184–189.